GERMAN-MONGOLIAN INSTITUTE
FOR RESOURCES AND TECHNOLOGY

The present work was submitted to Engineering Faculty

COPPER LEACHING MODELS AND SIMULATION

Bachelor Thesis

Submitted by: Sukhbaatar.B

Field of study: Raw materials and Process Engineering

Supervisor 1: Prof. Altangerel.L

Supervisor 2: M.Sc. Dorjsundui.G

Ulaanbaatar, May 7, 2019

Declaration of Authenticity

I certify that this thesis does not incorporate without acknowledgement any material previously submitted for a degree or diploma in any university; and that to the best of my knowledge and belief it does not contain any material previously published or written by another person where due reference is not made in the text.

Ulaanbaatar, May 7, 2019

Sukhbaatar.B

Acknowledgement

I would like to thank my supervisor Prof. Altangerel. L for accepting as his Bachelor student and guiding me throughout my thesis. He is always patient and willing to support me with helpful suggestions. I would also like to thank my co-supervisor, M.Sc. Dorjsundui. G, for his supervision. I am really grateful to all of my current classmates and instructors from GMIT, I have been receiving lots of help from them in these years. Particular thanks to Prof. Battsengel.B and Prof. Dr-ing. Bayanmunkh. M for sharing their knowledge and experience and helping me to solve the chemical and process problems. I also would like to thank Laboratory assistants Mr. Baasandorj. M and Mrs. Yaruunaa. T for supporting and helping on experiments. Special thanks to Achit Ikht LLC for supplying copper ore and sharing their knowledge. I really appreciate all of my family members and friends for their numerous supports and encouragements during my Bachelor.

Ulaanbaatar, May 7, 2019

Sukhbaatar.B

Abstract

In this thesis we deal with modeling and simulating the copper column leaching. The ore with 2.22% copper grade used in this study. Chalcopyrite ($CuFeS_2$) was main mineral in the test sample. Pyrite (FeS_2) was determined as the main gauge mineral of the sample. Three experiments produced with different flow rates which were $5.46l/h/m^2$, $10.25l/h/m^2$ and $16.4l/h/m^2$ with $3g/l$ sulfuric acid concentration (H_2SO_4) on column. Thus experiments were continued for 15 days. Thirty experiments produced with different acid concentrations for find right acid concentration for heap leaching. Comprehensive computational fluid dynamic (CFD) 'virtual 3D heap' was used as main model in the modeling and simulation. First prediction of this study was experimental and simulation results would be matched.

From vat leaching experiment, the best acid concentration were $4.5g$ (Figure 6.2) on heap leaching. We observed that solution flow rate and metal recover were directly depends each other from column leaching experiment. The simulation result was approximately matched with experiment result (Figure 6.8). The average simulaiton error was 0.6% (Table 6.5) which means our simulation was worked correctly.

Contents

List of Figures

List of Tables

1 Introduction

Copper is a chemical element and atomic number is 29 symbols with Cu. Only few metals can occur in natural in directly usable metallic form, one of them is Copper. Because of this property, humankind have used copper alloy since 4200 BC. Firstly, the copper used for making weapon, jewelry, armor coin, .etc. From 4200BC, humankind developed copper extraction to present.

1.1 Brief History

Mining and usage for the most metals dramatically increased the beginning of industrial revolution in the first half of 18th century. However, copper usage did not increased much until the growth of electricity. Because of copper properties, in 1866, a telegraph cable made of copper and connect North America and Europe; in 1878, Thomas Alva Edison produced an incandescent lamp powered through a copper wire [1]. After 100 years later from beginning of industrial revolution, the energy and telecommunications demand subsequently increased and that led to a huge growth in the demand for copper. In 2018, the construction industry is the largest single consumer about 47% of Copper alloys. The electronic products are 23%. Transportation is 10%. The consumer products are 11% and the industrial machinery is 9%. From 1965 to 2015, 50 years period, world copper production increased by 410% Table 1.1.

1.2 Copper Minerals and Origin of Copper

In nature, copper occurs in minerals as copper sulphides like chalcopyrite and chalcocite, the copper carbonates like azurite and malachite, and copper oxides like cuprit or native copper. Around 170 minerals contain copper, however only 10-15 minerals are economically efficient

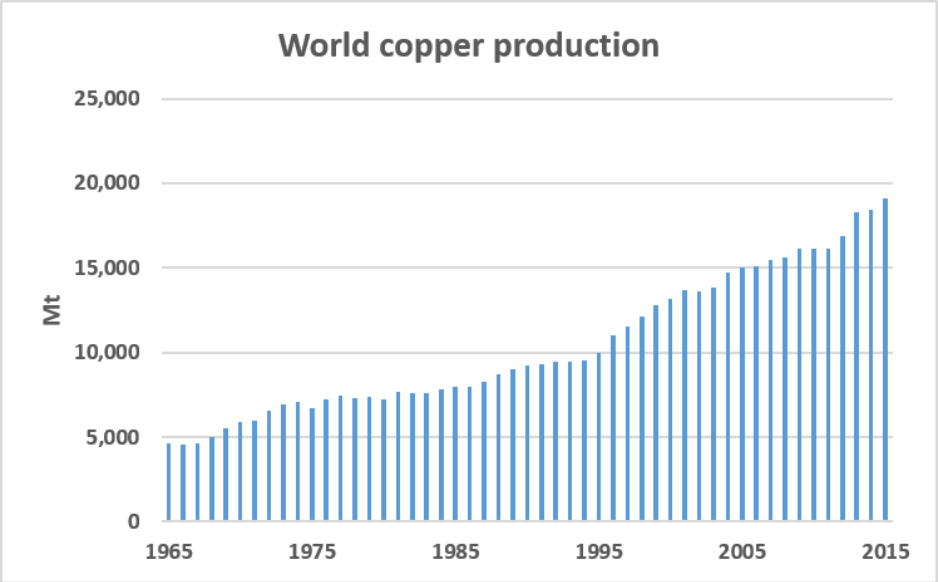

Tab. 1.1: World copper production from 1965 to 2015 [2].

to mine. The most important copper bearing minerals shown in Table 1.2.

Name	Formula	Copper %
Chalcopyrite	$CuFeS_2$	34.5
Chalcocite	Cu_2S	79.8
Covellite	CuS	66.5
Bornite	$2Cu_2S.CuS.FeS$	63.3
Tetrahedrite	$Cu_3SbS_3+x(Fe,Zn)_6Sb_2S_9$	32-45
Malachite	$CuCO_3.Cu(OH)_2$	57.3
Azurite	$2CuCO_3.Cu(OH)_2$	55.1
Cuprite	Cu_2O	88.8
Chrysocolla	$CuO.SiO_2.2H_2O$	37.9
Enargite	Cu_3AsS_4	48.41
Tennannite	$Cu_{12}As_4S_{13}$	51.6
Tenorite	CuO	79.75

Tab. 1.2: Copper bearing minerals

1.3 Technology Changes

The subsequent increased demand for all metals led to demand for new developing and efficiency technologies and process for mining. From humankind first used metals to now, Metal extraction process developed until became a science, which named Metallurgy.

After industrial revolution, there have been important innovations in mining techniques that enable to reduce production costs also to increase the resource reserves. The beginning of twentieth century, the two most important innovations discovered in short time. The first,

the mining engineer Daniel C. Jackling introduced the mass mining at the Bingham Canyon open-pit mine in Utah. Mass mining applied large-scale machinery in the production process, e.g., the use of steam shovels, heavy blasting, ore crushers, trucks and rail made profitable the exploitation of low-grade sulfide ores through economies of scale. In 1991, the second one was flotation process, created in Britain. Flotation process is used to concentrate sulfide ores and knowingly increase recovery rate of metal. After flotation process introduced, by 1935, metal recovery rate increased more than 90% from 75% in 1914.[1]

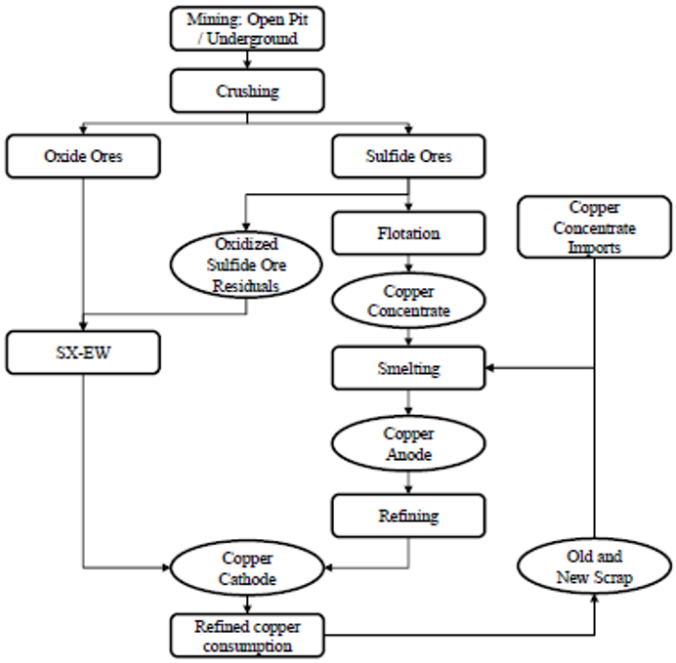

Fig. 1.1: Copper production technology "International Copper Study Group"

Once mass mining and flotation were introduced, world copper consumption significantly increased by five times, between 1900 and 1950, raising from 490Kt to 2490Kt. Because of that, sulfide ore's consumption increased and resource decreased.

Year by year, the fear of exhaustion increased but also study of resource reserves and technologies increased. Then, in 1968, the third important innovation discovered which was leaching techniques for oxide ores of Solvent-Extraction and Electro-Wining (SX-EW) at the Bluebird mine in Arizona. The leaching process is extracting substance from a solid by dissolving them in a liquid. In metal extraction process, leaching process's role is dissolve high-grade metal by applying acid solution to oxide ores. The SX-EW process presents a number of advantages compared with the more traditional pyrometallurgical process, e.g., it requires a lower capital investment and faster start-up times, allow to process lower grade ores and mining waste dumps [1]. The application of this process has spread greatly in recent decades. Between 1980 and 1995, the U.S. production by this method increased from 6% to

27%. The SX-EW has also spread at international level. In 1992, this process accounted for the 8% of the world production and by 2010, its participation increased to 20%. Current copper extraction scheme shown in Figure 1.1. [1]

Owing the current Industrial 4.0 revolution, SX-EW process integrated with monitor and feedback system, which is enable to evaluate the current process situation and control the whole process. In this regard, Computer and engineering science work together for forecasting metal recovery. Advantages of combination of computer and engineering science are save time, employments and money for reactant. In last decades, engineers and scientists worked on converting physical and chemical process to mathematical equation. Thus, almost all industrial processes can be simulated on computer program. In hydrometallurgical process, leaching simulation method was studied by certain scientists. The most efficient and precise method is Computational Fluid Dynamics (CFD) based method. Advantages of CFD are more factors included and more accurate than other method.

Mongolian biggest mining companies use pyrometallurgical process, which means these companies' have low concentrated sulfide and oxide ore dumps. Obviously, those dumps will be used for leaching and SX-EW in the future. Therefore, simulation models will be needed far more than today's in the future.

In this thesis, we are dealing with

1. Optimal parameters for the leaching
2. Behavior of the leaching process using the simulation tools
3. Study on realistic view of interconnection of business plan and leaching process via simulation.

Sample introduction

Hypothesis

Hypothesis of this thesis is using simulation program for predicting recovery rate and concentration of dump at any time.

Plan

Thesis experiment plan

Work plan	Work to do	2019														
		January				Febrary				March				April		
		I	II	III	IV	I	II	III	IV	I	II	III	IV	I	II	III
Prepare columns for leaching experiments	Column setup			■	■											
	Pump optimization			■	■											
	Prepare tanks for acid solution			■	■											
	Sample sort				■											
Sample preparation for experiments	Sample preparation for vat leaching				■											
	Prepare represent sample				■											
	Core sample sort				■											
	Crushing and miling on vat leaching sample				■											
Acid concentration optimization experiment on Vat leaching	Seive analysis on vat leaching sample				■											
	Element analysis on Sulfide and oxide ore				■	■	■	■	■							
	Chemical analysis on represent sample				■	■	■	■	■							
	Chemical analysis on samples of vat leaching					■	■	■	■							
Experiment preparation	Load sample on column									■						
	Prepare acid										■	■	■	■	■	
Flow rate optimization experiment on column leaching	Take sample from pregnant solution for each 12 hours										■	■	■	■	■	
	Refill acid solution tank every 12 hours										■	■	■	■	■	
	prepare acid solutions each 12 hours					■	■	■	■							
Result	Chemical analysis on samples of column leaching											■	■	■	■	■

Tab. 1.3: Experiment plan

2 State-of-Art

2.1 Copper mineralogy

Copper is mainly locate in the earth's crust as copper-iron-sulfide and copper sulfide minerals, such as chalcopyrite ($CuFeS_2$) and chalcocite (Cu_2S). The concentration of copper ore is low. Open pit mining uses more than 0.5% Cu ore and underground mining uses more than 1% Cu. Thus copper metal is produced from copper carbonates, oxides, hydroxy-silicates and sulfates by leaching, solvent extraction, and electrowinning Figure 2.2.

Primary copper minerals locates mainly in veins at deepest location among other copper minerals. Secondary copper minerals locates top of primary copper minerals also bottom of water table. Copper oxides and salts usually at oxide enrichment zone which is top layer of water table Figure 2.1.

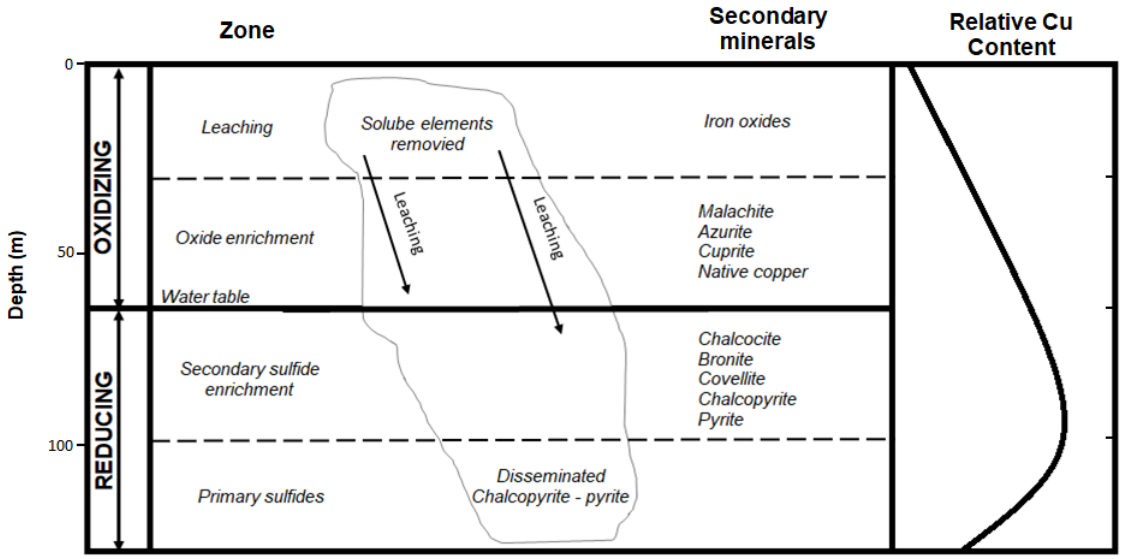

Fig. 2.1: Schematic diagram of a typical dump-leaching scenario.

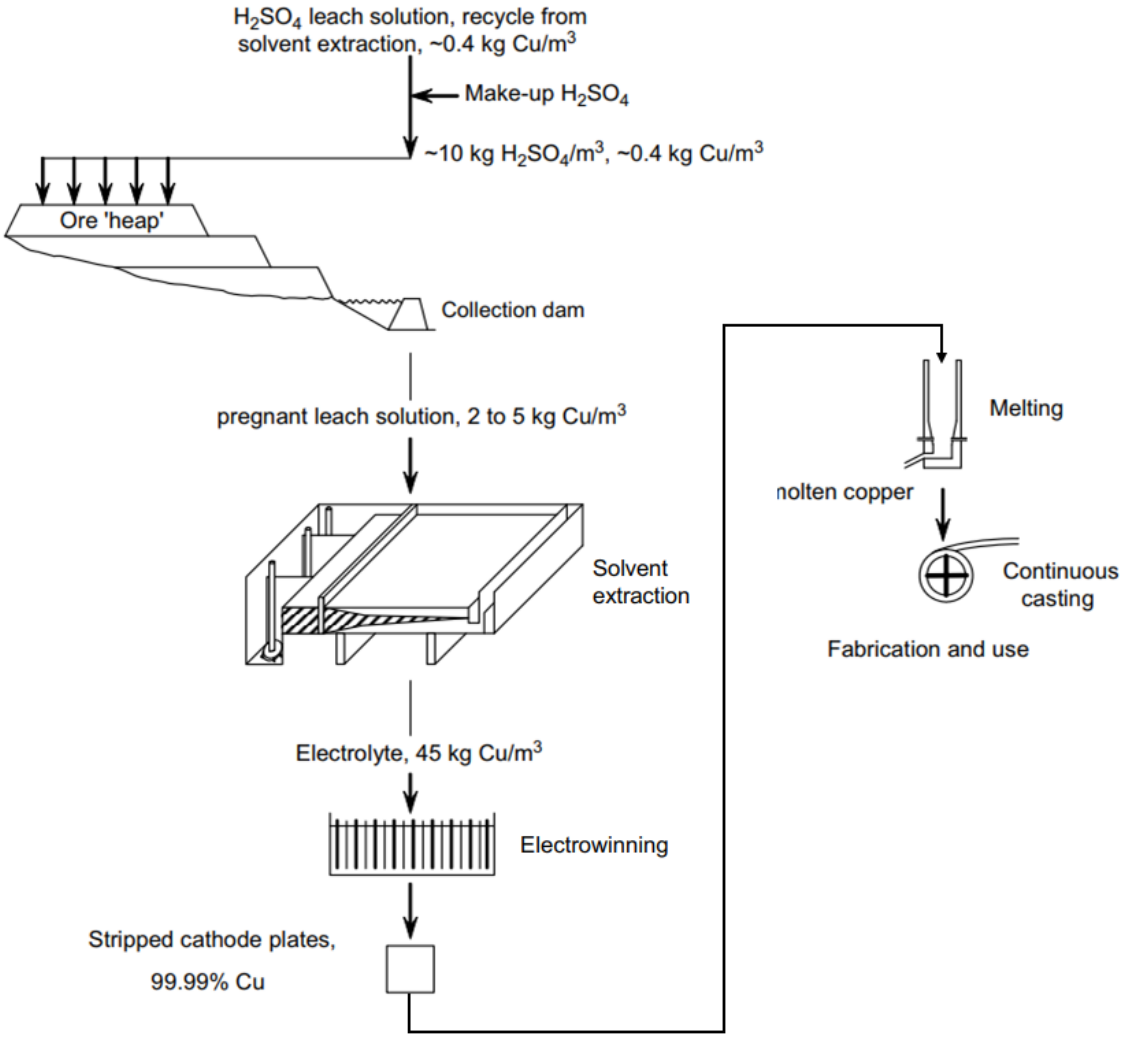

Fig. 2.2: Flowsheet for leaching oxide [3].

2.2 The Classification of Mineral grains

The mineral grains can be classified according to their accessibility to leach solutions, into five classes as illustrated in Table 2.1:

The metals concentration of pregnant solution significantly increases first few days. Because of metal position which is metal locates surface of rock Table 2.1.a. Then, recovery rate slowly increase, because metal locates inside of rock and connect to surface via pores or cracks Table 2.1.b and 2.1.c.

Table 2.1.d and 2.1.e do not contribute to the rate, at least in the early stages of leaching, but can become involved in the leaching process if, as a result of the prolonged contact with leach solutions, new cracks and fissures are generated in the gangue, thus making them accessible to leach solutions.

Classes	Illustration
(a) Grains exposed to the leach solutions at the surface of particles	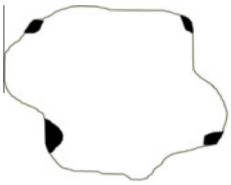
(b) Grains exposed to the leach solutions via pores or cracks	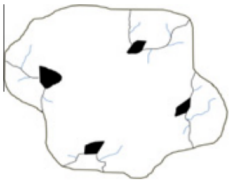
(c) Grains which become exposed to the leach solutions only after other grains have reacted	
(d) Grains from which pores or fissures that do not extend to the particle surface depart	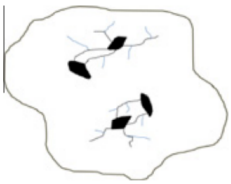
(e) Grains located inside the particles and not connected to a pore	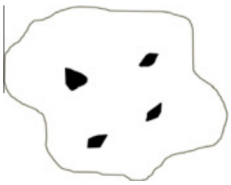

Tab. 2.1: the classification of mineral grains according to their accessibility of solutions [4].

2.3 Leaching

Copper heap and dump leaching can take place over a period of months to years. Copper leaching from low grade minerals and mine waste has become an important process in the mining industry. The large quantity of mining waste and low grade copper minerals represents a valuable resource. Copper ore grades are often too low to support the high cost of grinding and agitated leaching as indicated in Figure 2.3.

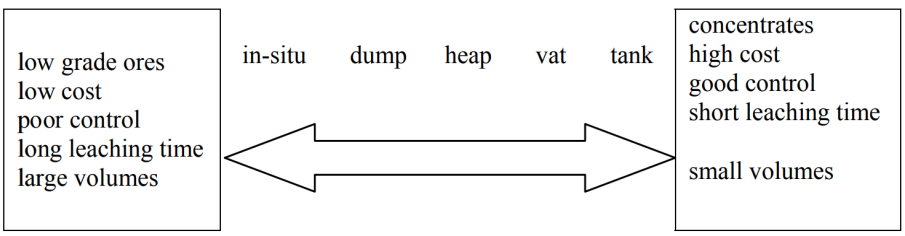

Fig. 2.3: Characteristics of different leaching techniques [5].

Dump leaching

Dump leaching is characterized by very low-grade ore leaching. It involves run-of-mine material that has not undergone significant crushing or processing. Dump leaching practice generally consists of dumping the low-grade run-of-mine material. The material is dumped over the edges of mining terrain under which a liner has been placed. It is sometimes placed on lined leaching pads. Leaching solutions are applied at the top of the dump and allowed to percolate through the dump. A schematic diagram of a typical dump is presented in Figure 2.4 . The action of the leaching solution may be amplified many times by bacterial activity in ores containing sulfides such as pyrite. [6]

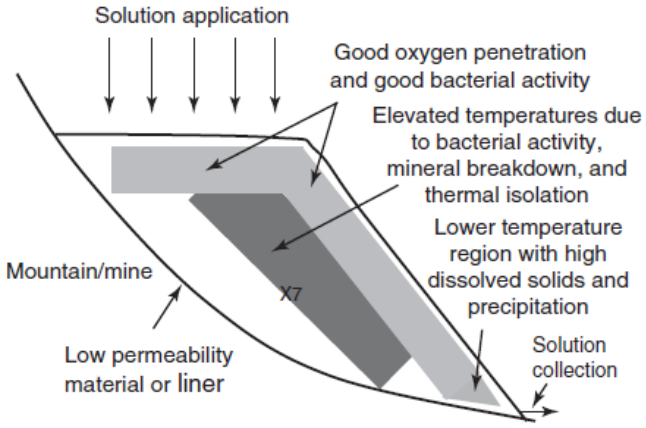

Fig. 2.4: Schematic diagram of a typical dump-leaching scenario.[6]

The bacteria that are naturally found on the ore particles can make a process economically feasible. In copper dump leaching, the solutions generally contain acid. In gold dump leaching, the solutions generally contain cyanide and hydroxide. The leaching solutions are then passed through a stripping process to concentrate the metal Table 2.2. The leaching solutions are combined with makeup leaching solution before being reapplied at the top of the dump. Some dumps are hundreds of feet deep. Dumps may take decades to leach. [6]

One of the most common ores that is leached in dumps is copper ore. Copper ore generally contains various copper oxides. In some locations, copper sulfide ores are leached. In most dump leaching operations, oxygen penetration is critical to the leaching process. Oxygen is used for chemical reactions.[6]

Heap leaching

Heap leaching is leaching performed on low to medium grade ores. The ores must have enough valuable material to justify additional size reduction. Most heap leaching operations are carried out on a much shorter timescale than dump leaching. Often the leaching time for ore such as simple oxides can be 45 days or less because of the high permeabilities, small particles, and shallow depths. However, for sulfide ores or larger run-of-mine material placed

Mineral	Chemical reaction
Tenorite	$CuO + H_2SO_4 \rightarrow CuSO_4 + H_2O$
Cuprite	$Cu_2O + H_2SO_4 \rightarrow CuSO_4 + Cu + H_2O$
Copper	$Cu + Fe_2(SO_4)_3 \rightarrow CuSO_4 + FeSO_4$
Azurite	$Cu_2(CO_3)_2 \cdot Cu(OH)_2 + 3H_2SO_4 \rightarrow 3CuSO_4 + 2CO_2 + 4H_2O$
Malachite	$CuCO_3 \cdot Cu(OH)_2 + 2H_2SO_4 \rightarrow 2CuSO_4 + CO_2 + 3H_2O$
Chrysocolla	$CuSiO_3 \cdot 2H_2O + H_2SO_4 \rightarrow CuSO_4 + SiO_2 + 3H_2O$
Atacamite	$2Cu_2(OH)_3Cl + 3H_2SO_4 \rightarrow 3CuSO_4 + CuCl_2 + 6H_2O$
Brochantite	$CuSO_4 \cdot 3Cu(OH)_2 + 3H_2SO_4 \rightarrow 4CuSO_4 + 3H_2O$
Antlerite	$CuSO_4 \cdot 2Cu(OH)_2 + 2H_2SO_4 \rightarrow 3CuSO_4 + 4H_2O$
Chalcanthite	$CuSO_4 \cdot 5H_2O \rightarrow CuSO_4 + 5H_2O$

Tab. 2.2: Copper oxide leaching reactions.[7]

Mineral	Chemical reaction
Chalcocite	$5Cu_2S + 4Fe_2(SO_4)_3 \rightarrow 4CuSO_4 + 8FeSO_4 + Cu_6S_5$
Blaubleibender	$Cu_6S_5 + 6Fe_2(SO_4)_3 \rightarrow 6CuSO_4 + 12FeSO_4 + 5S°$
Covellite	$CuS + Fe_2(SO_4)_3 \rightarrow CuSO_4 + 2FeSO_4 + S°$
Chalcopyrite	$CuFeS_2 + 2Fe_2(SO_4)_3 \rightarrow CuSO_4 + 5FeSO_4 + 2S°$

Tab. 2.3: Copper sulfide leaching reactions.[7]

Mineral	Chemical reaction
Pyrite	$FeS_2 + (1-6\beta)Fe_2(SO_4)_3 + 8\beta H_2O \rightarrow (3-12\beta)FeSO_4 + 8\beta H_2SO_4 + (2-2\beta)S°$
Calcite	$CaCO_3 + H_2SO_4 \rightarrow CaSO_4 \cdot 2H_2O + CO_2$
Siderite	$FeCO_3 + H_2SO_4 \rightarrow FeSO_4 + CO_2 + H_2O$
Limonite	$Fe_2O_3 \cdot 3H_2O + 3H_2SO_4 \rightarrow Fe_2(SO_4)_3 + 6H_2O$

Tab. 2.4: Important gangue leaching reactions in copper heap leaching.[8]

on leaching pads, leaching times may approach 600 days.[6]

Often, each lift or vertical section is less than 10 m high. These conditions allow much greater oxygen penetration than is commonly found in dump leaching. Shorter lifts often reduce compaction, reduce precipitation, and speed extraction. A general view of a heap leaching system is shown in Figure 2.5. Actual heap leaching operations are presented in Figure 2.6. In operations requiring large volumes of oxygen, air is injected at the bottom of the heap.[6]

The heap leaching lifts are constructed on top of pads. The pads often consist of foundation, underliner, liner, and overliner. Some pads contain additional layers as shown in Table 2.5. The additional layers are a liner and a drainage layer. Leak detection sensors are often placed in the drainage layer. Leak detection monitoring is often required for project

permitting.[6]

Pad construction begins with a properly formed foundation. The foundation must be smooth,

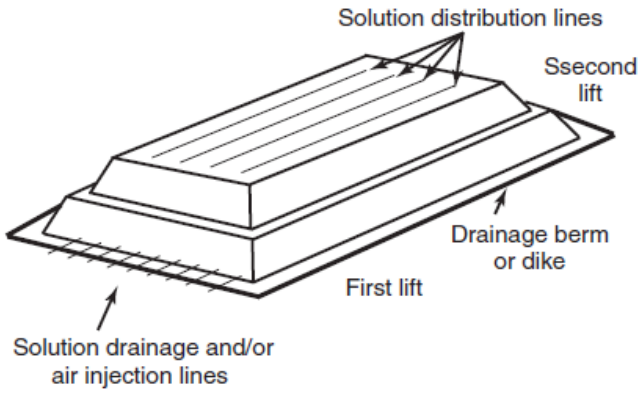

Fig. 2.5: Schematic diagram of a typical heap with two lifts[6].

Fig. 2.6: Examples of heap leaching operations[6].

compacted, and contoured for proper drainage. Contouring is often performed to direct fluid to a sump. The foundation is made of a variety of materials.

The permeability of the stacked ore is targeted to be at least 10 times greater than the

Ore layer: d_{80} around 15 mm, 10 m in depth per lift, permeability > 1 x 10^{-5} m/s
Overliner layer: intermediate size, d_{80} around 10 mm, around 30 cm in depth, permeability > 1 x 10^{-4} m/s, includes perforated pipes in many cases
Liner – LLDPE (linear low density polyethylene) or HDPE
Drainage layer: intermediate size, d_{80} around 5 mm, includes leak detection sensors, around 30 cm in depth, permeability > 1 x 10^{-4} m/s
Liner: LLDPE (linear low density polyethylene) or HDPE
Underliner: fine, d_{80} < 2 mm, low permeability < 10^{-8} m/s, often >30 cm in depth
Foundation – contoured for drainage, smooth

Tab. 2.5: Illustration of liner layers for heap and dump leaching [6].

application rate. Figure 2.7. show the effects of low, moderate, and excessive permeability on leaching using point source application. Note that excessive permeability results in channeling and nonuniform solution distribution when point source application is made.[6]

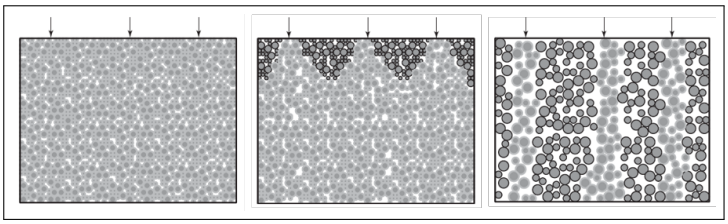

Fig. 2.7: Schematic diagram of point source (arrows) application of leaching solution using ore with low (left), moderate (middle) and excessive (right) permeability.[6]

2.4 Summary of the model functionality

Background

There is a rich history of heap and dump leach modeling work dating back to the early 1970s [9, 10, 11, 12]. Over the past three decades, along with the rapid advances in computational capability, a variety of options and approaches to heap leach modeling have been developed. These range from simple Excel spreadsheet-based approaches to the application of complex computational fluid dynamics (CFD) models using highly specialized, and often unique, software. However, not all of these methodologies are well-suited to metal production forecasting. For the purpose of this discussion, a tiered classification of models is consisted of Levels 1 through 6, with Level 1 as the simplest and Level 6 as the most complex (Table 2.6) [13].

Model level	Model type/functionality
1	Excel-based, no scale-up or time delays
2	Excel-based, empirical scale-up and time delays
3	Excel-based, in-heap inventory-adjusted production
4	Off-the-shelf heap modeling software
5	Phenomenological modeling
6	Advanced phenomenological modeling

Tab. 2.6: List of model types and functionality [13].

Selection of model properties

Marsden and Botz [13] introduced the advantages and disadvantages of different models and classify them into functionality levels; a summary is given in Table 2.7 [14]. Many scientists have been worked for developing different simulation approaches to enable precise forecast of heap leaching process. The first, simulation was a just spreadsheet, but now, simulation became complex phenomenological models [14].

Many scientists have been worked for developing different simulation approaches to eneable percise forecast of heap leaching process the simulation.

Comprehensive CFD 'virtual 3D heap' model is the most advanced modeling in 2019. Because this model uses more factors than other models and computational fluid dynamics (CFD). CFD manage fluid's unsaturated-saturated flow through porous by using mixed form of Richard's equation 3.4.

There are many different heap leaching models and modelling methods and difference are:

1. The function's primary variable such as cost analysis, metal recover, flow rate ,.etc.
2. Model's cost, accuracy and time constrain.

For choosing one method out of other methods, few requirments are matched the simulation.

1. What is the problem? What variable are needed? If primary variable is known, then more accurate function and algorithm able to be chosen.
2. Budget
3. How much time will be needed for simulation?

Model Level	1	2	3	4	5	6
Model Type	Spreadsheet No scale-up	Spreadsheet with scale-up	Spreadsheet scale-up and inventory adjustment	Mass-balance software	Fluid flow + chemical reactions	Comprehensive CFD 'virtual 3D heap'
Tonnes & grade of ore over time	✓	✓	✓	✓	✓	✓
Column leach data utilised	✓ Extraction curve	✓ With delay factor	✓ + scale-up factor	✓ + scale-up factor	✓ calibrate leach kinetics	✓ to calibrate leach kinetics
Solution inventory tracked		✓	✓	✓	✓	✓
Heap permeability			Scale-up factor	Scale-up factor	✓ dynamic by ore type	✓ dynamically, local, depth & time
Gas-liquid flow				✓	✓	✓
Solution channelling			Discount factor	Discount factor	✓	✓
Oxidation					✓	✓
Particle kinetics					✓	✓
Thermodynamics					✓ reactions	✓ + liquid-solid-gas
Bacteria					✓	✓
Gangue reactions						✓
Precipitation						✓
Meteorological rain, evaporation, temperature					✓	✓ + internal liquid freezing

Tab. 2.7: Summary of the model functionality [14].

In thesis work, we introduce column leaching copper recovery forecast with advanced phenomenological which was level 6 modeling in Table 2.7. However, these models (Table 2.7) are for forecasting metal recovery of heap leaching, so that we used Comprehensive CFD 'virtual 3D heap' model type except heap permeability, gas flow, oxidation , thermodynamics, bacteria, precipitation and meteorological rain, and evaporation approaches.

3 Methodology

3.1 Experimental Method

Sample preparation

Jaw, roll crushers and ball mill were used for crushing and milling process. Coning and quartering method was used for dividing the copper ore sample. Coning and quartering is a method used by analytical chemists to reduce the sample size of a powder without creating a systematic bias. The technique involves pouring the sample so that it takes on a conical shape, and then flattening it out into a cake. The cake is then divided into quarters. Each quarters are same particle size and concentrate.

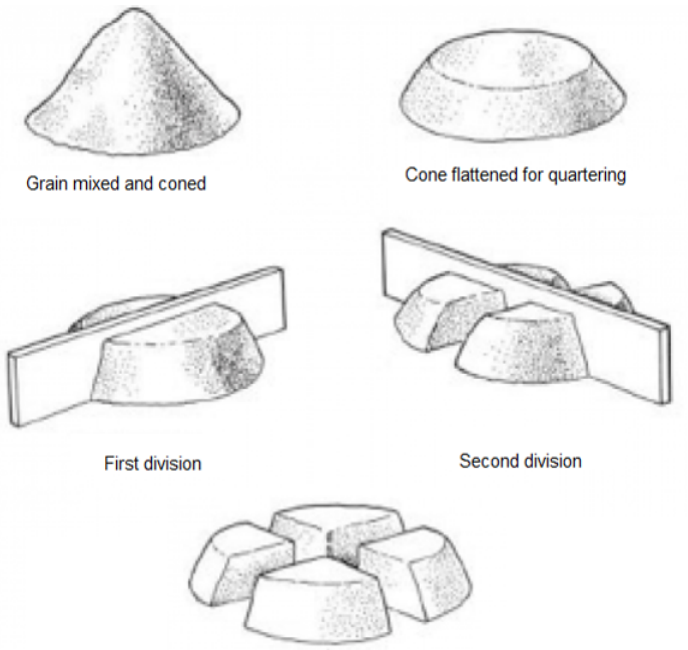

Fig. 3.1: Coning and quartering method[15].

Vat leaching

Vat leaching is simple and efficient mode of effecting adequate contact beween the solute and aqueous solvent. It utilizes the counter-current principle, with the ore to be leached remaining stationary, as differentiated from most counter-current methods, where all materials moving. The ore, confined in cylinder leaching vat is successively treated with an increasing concentration of leach solution when mixing solution. Vat leaching can be based on both continuous batch reactor and batch reactor. In this thesis, batch based vat leaching was selected, due to equipment properties.

Filtration method was used for taking aqueous sample. There are several filtration methods: simple or gravity, hot and vacuum filtrations. The selection of the appropriate method is typically dictated by the nature of the experimental situation. Solid particles were ultra-fine in solution. Regular filtration (gravity filtration) was very slow to filtrate, so gravity filtration method used in filtration. In a vacuum filtration, the solution to be filtered is drawn through the filter paper by applying a vacuum to a filter flask with a side arm adaptor (also known as a Buchner flask). Vacuum filtration is typically a fast and efficient way of filtering. This method typically comprises a Büchner funnel fitted with the "—" size filter paper and a vacuum applied to the side arm of the filter flask.

Fig. 3.2: Büchner funnel (left) and filter flask (right).

3.2 Computational Method

The leaching model has been implemented within an in-house multi-physics computational fluid dynamic (CFD) framework. The computational procedure employed for the solution of unsaturated-saturated flow through the porous media is based on the mixed form of the classical Richards' Equation (3.3). CFD model structure and coupling is shown in Figure 3.3.

Flow in porous media

Flow through variably saturated porous media is characterized by the classical Richards equation combined the pressure head and the moisture content of the porous medium. There are three standard forms of the Richards equations: h-based (pressure head), θ based (moisture content) and 'mixed' form, where both variables are employed:

1. When the pressure head h is primary variable, Richards' equation has the following form

$$C(h)\frac{\partial h}{\partial t} = \nabla[K(h)\nabla h] + \frac{\partial K(h)}{\partial z} + S \tag{3.1}$$

In equation (3.1), h is solution pressure head, $K(h)$ is the hydraulic conductivity described as a function of pressure head, z is the direction of gravity, t is time and S is a source term, which also includes the boundary conditions [16].

$C(h)$ is the specific moisture capacity and defined as the following form

$$C(h) = \frac{\partial \theta}{\partial h} \tag{3.2}$$

In equation (3.2), θ is a moisture content defined as the volume of liquid/ total volume of solid-liquid-air space.

The h based form can be written in both unsaturated and saturated condition. However, this form gives highly mass-balance error, because of time derivative terms'. While $d\theta/dt$ and $C(h)(dh/dt)$ are mathematically equal in the continuous partial differential equation, but their analogues are not[17].

2. When the pressure head θ is a primary variable, Richards' equation has the following form

$$\frac{\partial \theta}{\partial t} = \nabla[D(\theta)\nabla\theta] + \frac{\partial K(\theta)}{\partial z} + S \tag{3.3}$$

where $D(\theta)$ is hydraulic diffusivity. Comparing to the h based formulation θ has perfectly mass conservative discrete approximations can be applied. However, this form can be written in only saturated condition.

3. The mixed form of Richards' equation is for solving model of the variably saturated liquid flow through the porous media with lower mass-balance error and can be written in both unsaturated and saturated flow. In this equation, airflow in liquid is assumed

to be minimal and gas flow does not affect liquid flow but fluid flow can influence the gas movement[16, 17].

$$\frac{\partial \theta}{\partial t} = \nabla[K(h)\nabla h] + \frac{\partial K(h)}{\partial z} + S \tag{3.4}$$

In solution of equation (3.4) requires relationships for pressure head – liquid content - hydraulic conductivity to be specific to describes the moisture characteristic of the porous media. The unsaturated moisture content $\theta(h)$ and hydraulic conductivity $K(h)$ are nonlinear functions of the pressure head and are represent here, Equations (3.5) and (3.6) by the van Genuchten-Maulem model[16].

$$\theta(h) = \begin{cases} \theta_{res} + \dfrac{\theta_{sat}}{\theta_{res}}\left[1 + |\alpha h|^n\right]^m, & h < 0 \\ \theta_{sat}, & h > 0 \end{cases} \tag{3.5}$$

$$K(h) = K_{sat}\left[\frac{\theta(h) - \theta_{res}}{\theta_{sat} - \theta_{res}}\right]^L \times \left[1 - \left(1 - \left[\frac{\theta(h) - \theta_{res}}{\theta_{sat} - \theta_{res}}\right]^{\frac{1}{m}}\right)^m\right]^2 \tag{3.6}$$

where θ_{sat} is the saturated moisture content, θ_{res} is the residual moisture content, L is a pore tortuosity/connectivity dimensionless parameter normally assumed to be 0.5, but is often negative when empirically fitted. Schaap and Leij [18] found that to insure a physically realistic relationship the constraint $L > -2/(n-1) - 2$ should be employed, α is related to the inverse of the air-entry pressure, n is a measure of the pore-size distribution and $m = 1 - \frac{1}{n}$.[16]

The equation for the solute transport in the porous media is

$$\frac{\partial(\theta C_i)}{\partial t} - \nabla(\theta D_{i,jk}\nabla C_i) + \nabla(qC_i) = S_i + S_i^{cl} \tag{3.7}$$

q is where defined as follows

$$q = -K(h)\nabla H \tag{3.8}$$

and

$$H = h + z \tag{3.9}$$

In Equation (3.7), C_i is the concentration of species i in the solution phase, q is the darcy flux , $_{ijk}$ are (x,y,z) directions, S_i the production or consumption of the species i and S_i^{cl} is the moles of species entering or leaving preferential paths, H is total hydraulic head and $S_i^{cl} = S^{cl}\theta C_i$. The dispersion coefficient $D_{i,jk}$ is dependent upon the velocity components and longitudinal and transverse dispersivities (Equation (3.8)) [16]. The dispersion coefficient is often estimated from experimental data or derived from a relationship between the solute transport work given in this paper.

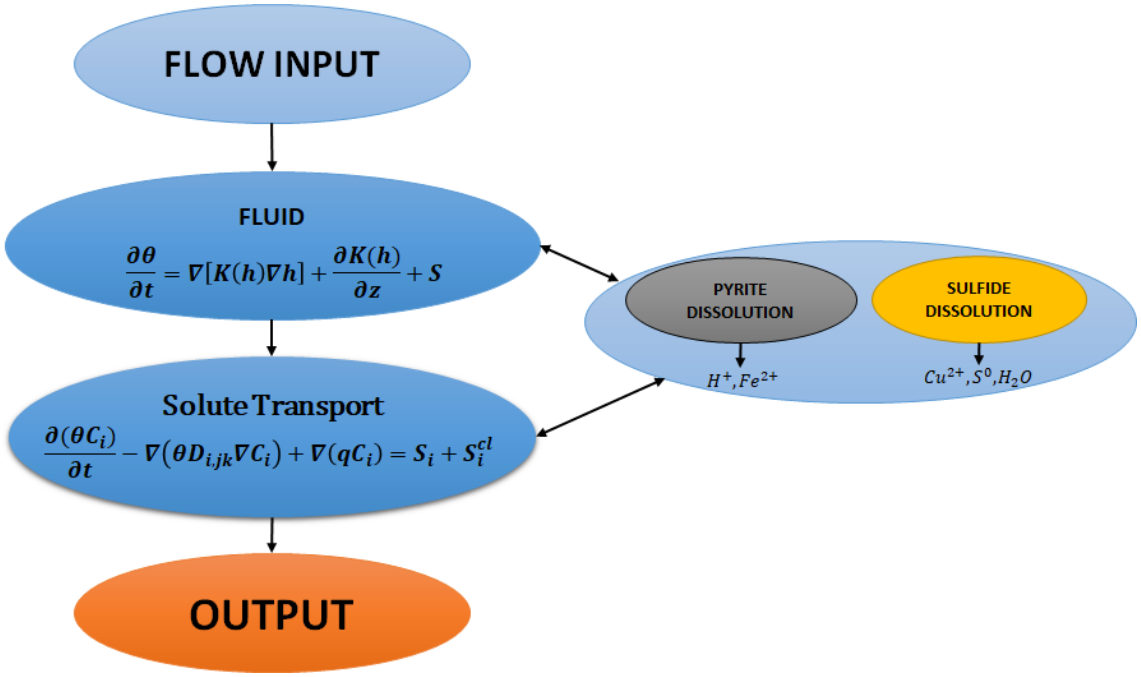

Fig. 3.3: CFD model structure and coupling.

3.3 Leach Kinetics

The principle mineral reactions in the ore modeled in this thesis are chalcopyrite ($CuFeS_2$) and pyrite (FeS_2). The shrinking core model is applied to each particle size distribution.

Pyrite Dissolution

The pyrite dissolution chemical reaction has the following form

$$FeS_2 + 14Fe^{3+} + 8H_2O \longrightarrow 15Fe^{2+} + 2SO_4^{2-} + 16H^+ \tag{3.10}$$

Kinetic rate is defined by Arrhenius equation has the following form

$$\frac{d\beta_p}{dt} = \frac{R_A 601.5[Fe^{3+}]}{r_p \zeta [Fe_{tot}][H^+]^{0.4}} e^{\frac{-10317}{T}} \tag{3.11}$$

In equation (3.11), β_p is the fraction of pyrite reacted, r_p is the pyrite grain radius(m), ζ is the particle shape function, T is the temperature (K) and R_A is a rate constant based on known data.

Chalcopyrite Rate Kinetics

The Chalcopyrite dissolution chemical reaction is

$$CuFeS_2 + 4Fe^{3+} \longrightarrow Cu^{2+} + 5Fe^{2+} + 2S^0 \tag{3.12}$$

Kinetic rate (Equation (3.15)) is defined by combination of Arrhenius-type equation (Equation (3.13)) and Gibbs free energy (Equation (3.14)).

Arrhenius-type equation has the following form

$$\frac{d\beta_c}{dt} = \frac{R_A t_e \sigma \triangle G}{\rho_b r_p^2 e^2} \frac{(1-\beta)^{1/3}}{[1-(1-\beta)^{1/3}]} \tag{3.13}$$

Gibbs free energy ($\triangle G$) of reaction as defined as follows

$$\triangle G = R_A T \ln \frac{[Fe^{2+}]^{5/4}[Cu^{2+}]^{1/4}}{[Fe^{3+}]} \tag{3.14}$$

Combining Equation (3.13) and (3.14) gives Kinetic rate (Equation (3.15)) of chalopyrite.

$$\frac{d\beta_c}{dt} = R_A \frac{T e^{0.0735 R_B T}}{r_p^2 \zeta} \ln \frac{[Fe^{2+}]^{5/4}[Cu^{2+}]^{1/4}}{[Fe^{3+}]} \frac{(1-\beta)^{1/3}}{[1-(1-\beta)^{1/3}]} \tag{3.15}$$

3.4 Solid-Liquid Dissolution

A key aspect of the column leach process is the dissolution of metals from the minerals of interest. in this work, the rate of dissolution is calculated by using shrinking core model to combine the effects of diffusion through the rock matrix and the kinetic reaction rates. The shrinking core equation is solved for each mineral in each characteristic particle size at each point in time. In this way, the ore material can be characterized by defining a particle size distribution, with each particle size class having its own initial head grade. The equation (3.16) used to calculate the rate of diffusion of a mineral is solved explicitly for each particle

size at the start of each time step.

$$\frac{dr_m}{dt} = -\frac{3r_m}{4\pi r_0^2}\frac{M_i}{\rho_{ore} x_i}\frac{D_{eff} c_0 A_m}{[3D_{eff} r_0 c_0 + 2(r_0 - r_m) r_m^2 (1-\varepsilon_p) A_m]} \tag{3.16}$$

In equation (3.16), r_m is the current mineral radius, r_0 is the initial particle radius, A_m comes from the kinetic rate equation for the current mineral, c_0 is the concentration of available reactant at particles surface, D_{eff} is the effective rock diffusion coefficient, ε_p is the rock void age, ρ is the ore density, M_i is the molecular weight of the mineral and x_i is the mass fraction of the mineral[14].

The value of A_m comes from the general expression for the kinetic rate equations, such as those produced by [16], and the general form for which is

$$A_m = \frac{d\beta}{dt} = Ae^{\frac{-B}{RT}}, \tag{3.17}$$

where β is the fraction of mineral reacted and A,B are functions of the individual kinetic rate equation.

4 Experiment Procedure

4.1 Sample preparation

The sample were crushed until -38mm by Jaw crusher. Because core samples could not represent dump particle size and for dividing equal size Figure 4.1. After crushing process, the main sample were divided into four parts by using coning and quartering method Figure 3.1. The first three parts were loaded into column for leaching experiment and the last part was represent sample. The column dimension is 2m high, inner diameter was 23cm, and outer

Fig. 4.1: before (left) and after (right) crushing process.

diameter was 24 cm. the bottom of column were filled with quartz and height was 9cm. The sample height was 160cm. Glass wool pad were covered the sample for saturated acid flow Figure 4.2. Mass of each column shown in Table 4.1.

	Column 1	Column 2	Column 3
Mass (kg)	97.991	100.815	100.735

Tab. 4.1: Net sample mass in columns

The coning and quartering method used twice on represent sample for dividing sixteen parts Figure 4.3.

Fig. 4.2: Column with sample

Around 540g sample was taken from each part for element and phase analysis test. The analysis test sample was 8.715kg. Eight parts sample were used sieve analysis. Two parts 20kg sample were crushed then milled for vat leaching experiment and rest were stored as a represent sample.

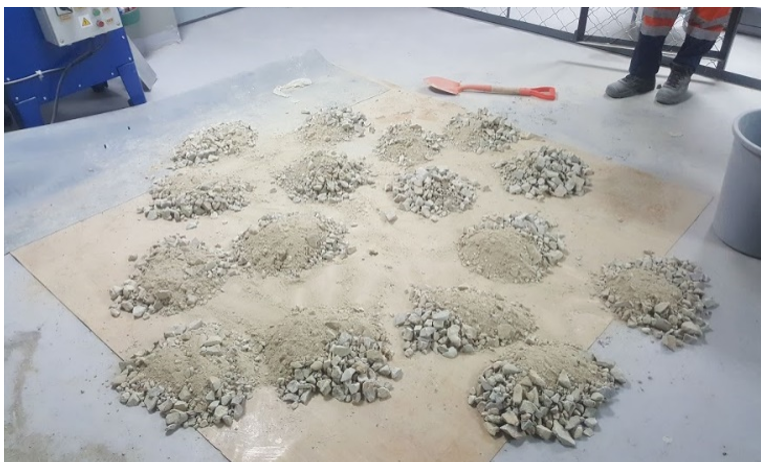

Fig. 4.3: Using after coning and quartering method.

Crushing and Milling procedure

In sample preparation, there were two parts for crushing, the first was for dividing equal particle size, and the second was for preparing sample of vat leaching. In second part of crushing procedure, jaw crusher was used as a primary crusher. Standard maximum inlet feed particle size of laboratory jaw crusher is 100mm or below. Maximum particle size of discharge/product is 38mm and minimum is 8mm. 20kg of sample were crushed by primary crusher until -8mm. The roll crusher was used as a secondary crusher. The roll crusher used discharge of jaw crusher as a feed and crushed until –mm. Ball mill was used as a miller. Ball mill's feed was 10kg crushed sample with 20L water. Thus, the sample was milled for 60 minutes. Equipment shown in Figure 4.4.

Sieve analysis

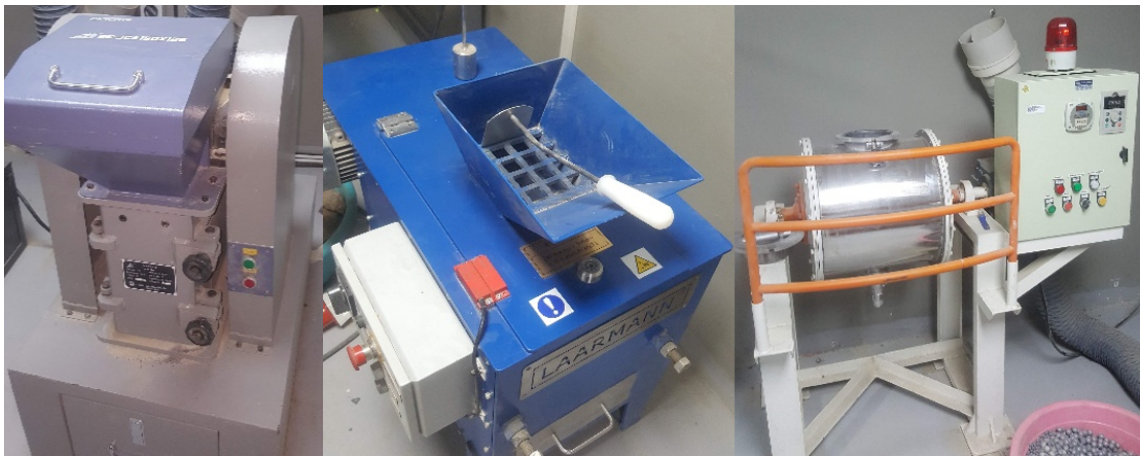

Fig. 4.4: From the left: Jaw, Roll crushers and Ball mill.

A different size of laboratory sieves and mechanical sieve vibrator Figure 4.5 used for sample preparation and sieve analysis test of sample. I did two types sieve analysis, first was on coarse sample, which was a feed of column leaching and second was on fine sample, which was a feed of vat leaching. On the coarse sieve analysis used sieve sizes of 12.5mm, 8mm, 4mm, 2mm, 1mm, 0.5 mm, 0.25mm, 0.125mm and 0.063mm. On the fine sieve analysis used sieve sizes of 1mm, 0.5 mm, 0.25mm, 0.125mm and 0.063mm.

4.2 Vat leaching

Purpose of vat leaching experiment is optimize acid concentration with highest metal recovery. Experiment acid range was from $2g/l$ to $9g/l$ and period was $0.5g/l$. Thus each samples were $500g$ of milled sample from represent sample. We did parallel test on each experiment, thus total number of experiment was 30. Each experiments test duration was 90min and mixer

Fig. 4.5: Mechanical sieve vibrator and sieves.

speed was 3000rpm at 25 degree of Celsius. Equipment shown in Figure 4.6. Aqueous samples were taken from each experiments by filtering methods. The element analysis for sample at "Khan Lab LLC".

Fig. 4.6: Vat leaching tank and mixer

4.3 Pump

Pump introduction

"PJLM1501 PVDF series diaphragm metering pump" (Figure 4.7) was used on column leaching experiment. Maximum flow rate of pump was $15L/h$ and head pressure was $1Bar$. Pump had not flow rate insert system but it has level insert system. Pump had 100 levels and we can change percent of each level.

Pump calibration

Our aims of each pump's flow rate were $5l/h/m^2$, $15l/h/m^2$ and $10l/h/m^2$. We measured time which was pump fill $100ml$ volumetric flask by solution for calibrate. The first pump filled $100ml$ volumetric flask by $30min$ which means flow rate of solution was $200ml/h$. The second pump filled $100ml$ volumetric flask by $10min$ which means flow rate of solution was $600ml/h$. The third pump filled $100ml$ volumetric flask by $16min$ which means flow rate of solution was $375ml/h$. When pumps flow rates transferred to heap leaching flow rate, first pump flow rate $5.46l/h/m^2$, $16.4l/h/m^2$ and $10.25l/h/m^2$. Our aims and results were approximately matched.

Fig. 4.7: Pump

4.4 Column leaching

Column leaching purpose was determine parameters and flow rate optimization for simulation. Column leaching used $3g/l$ acid concentrated solution. Three columns were used for leaching and each of them had different flow rates.

First we prepared $3g/l$ concentrated solution and poured to acid solution tank. The experiment run continuously for 15 days, so that acid solution tank were filled continuously. Each pumps were calibrated as mentioned in "Pump calibration" part. The bottom of columns were filled with quartz for precipitating fine particles on bottom of quartz and taking pregnant solution from top of quartz Figure 4.8. The top of columns were covered by glass-wool pad for creating saturated flow and condensing vaporized acid solution Figure 4.9.

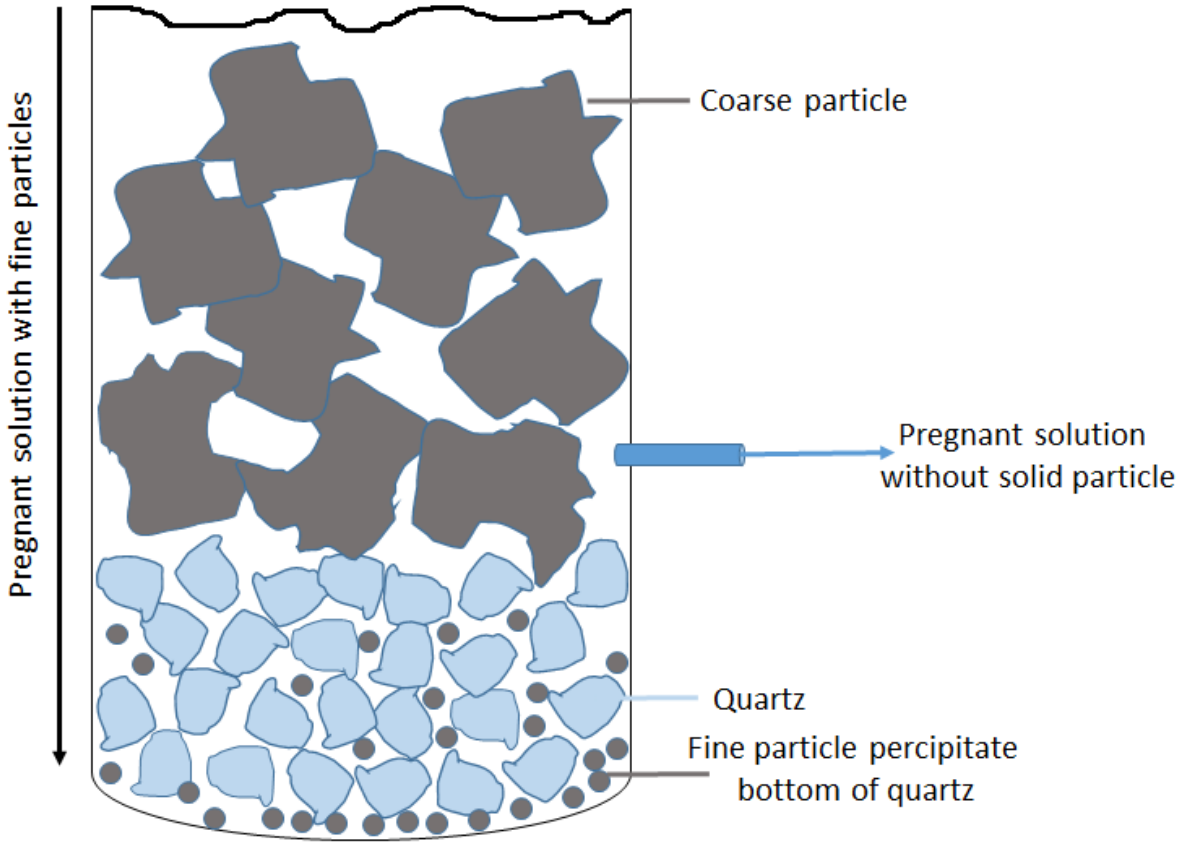

Fig. 4.8: Quartz principle

Experiments were started 1am of $29^{th} March, 2019$ and first pregnant solution was discharged at 7pm of $29^{th} March, 2019$ from column that had highest flow rate. Every 12 hours, 9am and 9pm, samples were taken from pregnant solution tanks and acid solution tanks were

refilled by new acid solutions.

After took sample from pregnant solution tank, we measured volume of the pregnant solutions and dischared to discharge tank. Then, pregnant solutions were mixed with sodium hydroxide ($NaOH$) for neutralizing and discharged Figure 4.10.

Neutralizing chemical equation is Equation (4.1).

$$H^+ + OH^- \longrightarrow H_2O \tag{4.1}$$

After measure volume of each columns' pregnant solution, mix and sum volume of all preg-

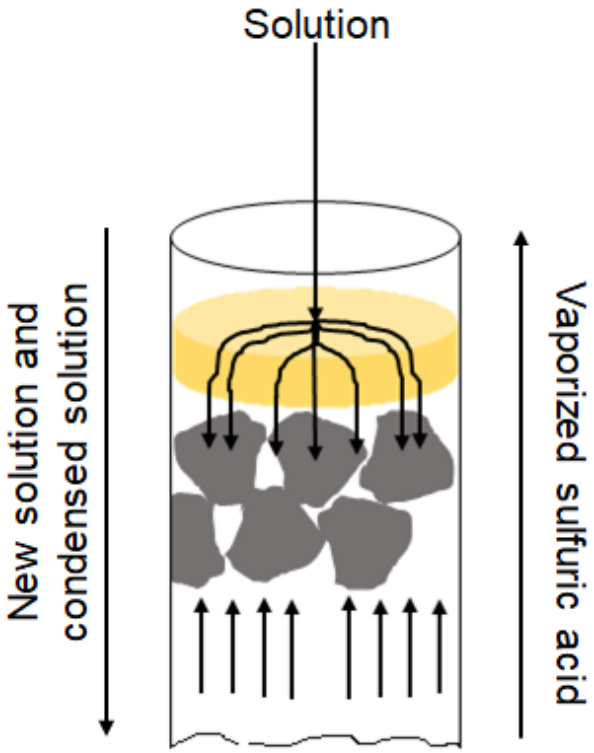

Fig. 4.9: Glass-wool principle

nant solution in discharge tank. From the volume of pregnant solution calculate amount of sodium hydroxide and mix with pregnant solution. For checking the pH of solution in discharge tank used pH indicator paper. When pH indicator paper present color of 7 pH, solution was discharged.

The element analysis for samples at "Central Geological Laboratory of Mongolia".

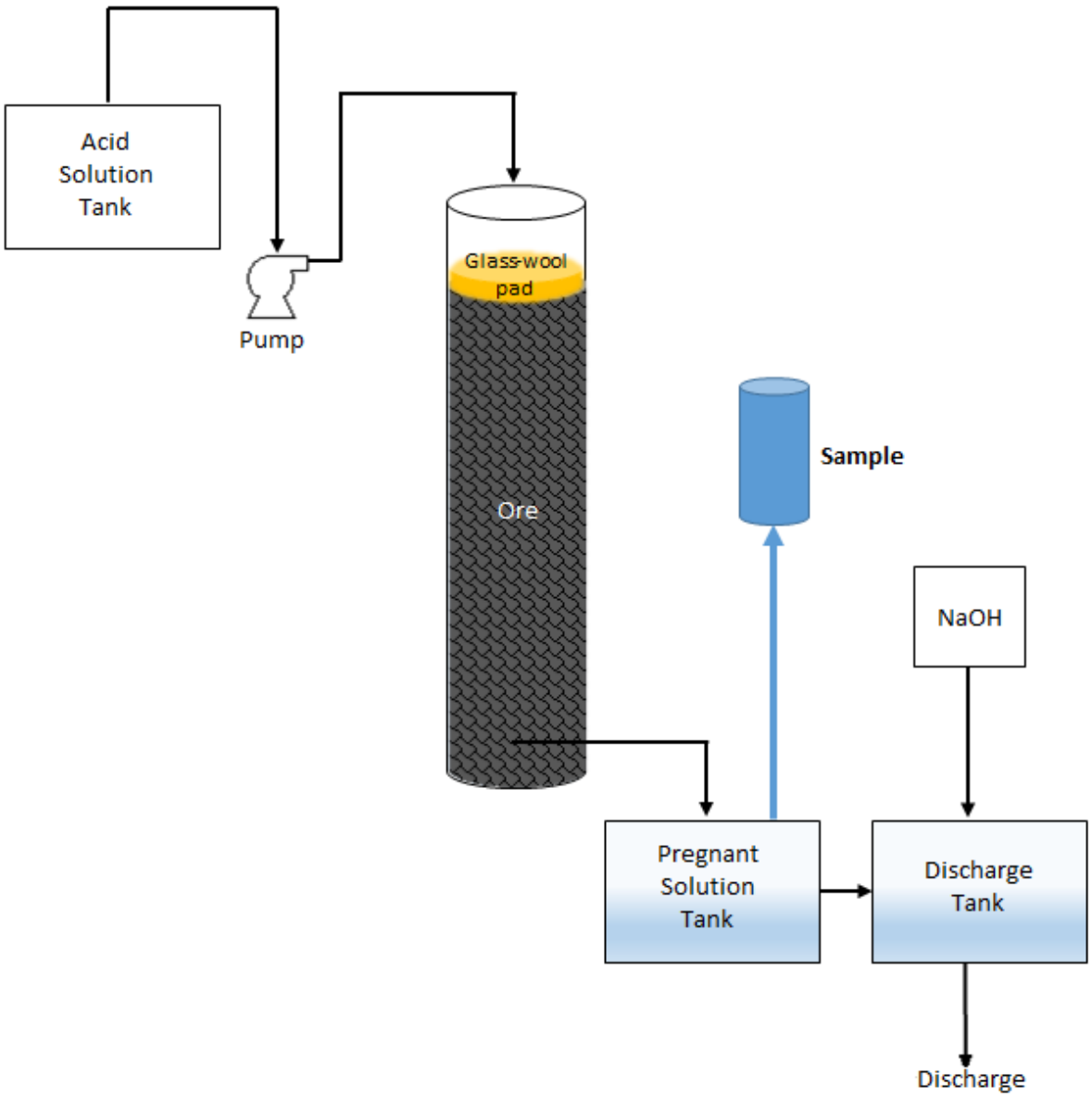

Fig. 4.10: Flow-sheet of column leaching experiment

5 Simulation

Column 3D model was drawn by AutoCad 2019 software Figure 5.1.

Fig. 5.1: Column 3D model

CFD model for a leaching is implemented via Finite Volume Method (FVM) algorithm (Figure 5.3). Firstly liquid phase was modeled and simulated with Richards equation (Figure 3.3). And then each instant, dissolution rate of the mineral observed by the kinetics of several ores under different particle size.

The 3D model was discretized into meshes by T3D mesh generator Figure 5.2

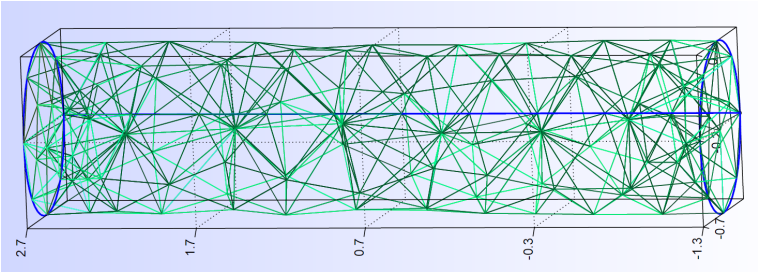

Fig. 5.2: Column 3D discretization model

The column geometry was meshed employing 63258 hexahedral elements. Each element was approximately $1cm^3$. This is a normal mesh size and it will allow a number of scenarios to be investigated employing the virtual column on a standard pc with in a reasonable time period. A fixed flux boundary condition was applied to the active leaching surfaces, meteorological

data was applied transiently to all external surfaces and the bottom surface was set to a free drainage condition. Further details of solution algorithm was givin in [19].
Model validation has done by column leaching experiment of 15 days took approximately 12 hours to run. The forecast of Copper and Iron recovery highly accurate and it is enables to estimate the recovery in long term under different conditions.

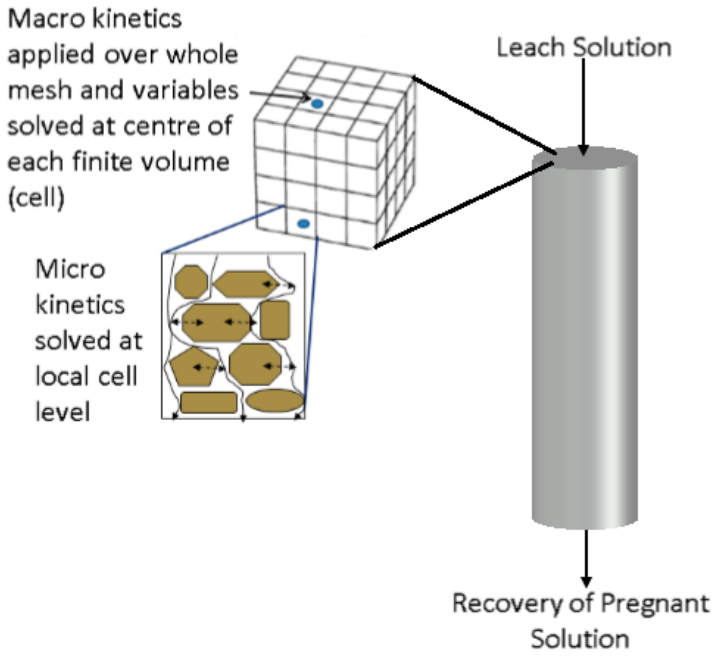

Fig. 5.3: Mesh of column, macro and micro solution points and boundary conditions.

6 Experimental and Simulation Results

6.1 Sieve analysis

The eight samples were analyzed by sieve analysis and results were presented in Table 6.1, 6.2 and Figure 6.1. From the Gaudin-Schumann curve (Figure 6.1), we considered every columns had same fraction sizes and same masses of each particle sizes. Which means, on simulation, We can consider our columns initial parameters were exactly same.

	Sample 1			Sample 2			Sample 3			Sample 4		
Sieve size	Mass (g)	Passing %	Retained %	Mass (g)	Passing %	Retained %	Mass (g)	Passing %	Retained %	Mass (g)	Passing %	Retained %
12500	1885.4	62.92	37.08	2919.6	50.16	49.84	2439.3	55.34	44.66	1314.7	69.67	30.33
8000	552.9	52.04	10.87	660.0	38.89	11.27	485.2	46.46	8.88	455.2	59.16	10.50
4000	660.7	39.05	12.99	601.1	28.63	10.26	567.1	36.08	10.38	559.5	46.25	12.91
2000	453.4	30.13	8.92	396.3	21.87	6.77	436.9	28.08	8.00	430.2	36.33	9.93
1000	403.9	22.19	7.94	337.6	16.10	5.76	400.9	20.74	7.34	402.4	27.04	9.28
500	316.2	15.97	6.22	263.6	11.60	4.50	315.5	14.96	5.78	326.0	19.52	7.52
250	244.9	11.15	4.82	199.8	8.19	3.41	246.2	10.45	4.51	252.3	13.70	5.82
125	293.0	5.39	5.76	206.3	4.67	3.52	257.0	5.75	4.71	234.7	8.28	5.42
63	162.9	2.19	3.20	200.2	1.25	3.42	211.4	1.88	3.87	287.8	1.64	6.64
-63	111.2	0.00	2.19	73.5	0.00	1.25	102.6	0.00	1.88	71.2	0.00	1.64
Total	5084.5		100	5858.0		100	5462.1		100	4334.0		100

Tab. 6.1: Sieve analysis data of sample one to four

6.2 Vat leaching

Vat leaching experiment results were shown in Table 6.4 and Figure 6.2. Relationship between sulfuric acid and copper recovery was directly depend each other. Which means, when acid concentration increased, copper recovery increase. But, acid concentration can not be increased up to $5g/l$ because of environmentally and economically efficient. Another reason is iron. As you can see from Figure 6.2, difference between copper and iron concentration was

	Sample 5			Sample 6			Sample 7			Sample 8		
Sieve size	Mass (g)	Passing %	Retained %	Mass (g)	Passing %	Retained %	Mass (g)	Passing %	Retained %	Mass (g)	Passing %	Retained %
12500	4982.9	39.39	60.61	2951.1	51.87	48.13	2889.1	43.56	56.44	3192.2	46.51	53.49
8000	678.6	31.14	8.25	542.3	43.02	8.85	553.7	32.74	10.82	646.5	35.67	10.83
4000	692.8	22.71	8.43	662.2	32.22	10.80	469.4	23.57	9.17	573.8	26.06	9.62
2000	437.9	17.39	5.33	443.4	24.99	7.23	292.4	17.86	5.71	369.8	19.86	6.20
1000	372.2	12.86	4.53	396.6	18.52	6.47	239.2	13.19	4.67	311.1	14.65	5.21
500	295.1	9.27	3.59	316.8	13.35	5.17	182.9	9.61	3.57	242.0	10.59	4.06
250	227.3	6.51	2.76	241.5	9.41	3.94	141.7	6.85	2.77	182.3	7.54	3.05
125	240.8	3.58	2.93	232.6	5.62	3.79	137.2	4.17	2.68	190.5	4.34	3.19
63	254.2	0.49	3.09	225.6	1.94	3.68	181.7	0.62	3.55	211.0	0.81	3.54
-63	39.9	0.00	0.49	119.0	0.00	1.94	31.5	0.00	0.62	48.2	0.00	0.81
Total	8221.7		100	6131.1		100	5118.8		100	5967.4		100

Tab. 6.2: Sieve analysis data of sample five to eight

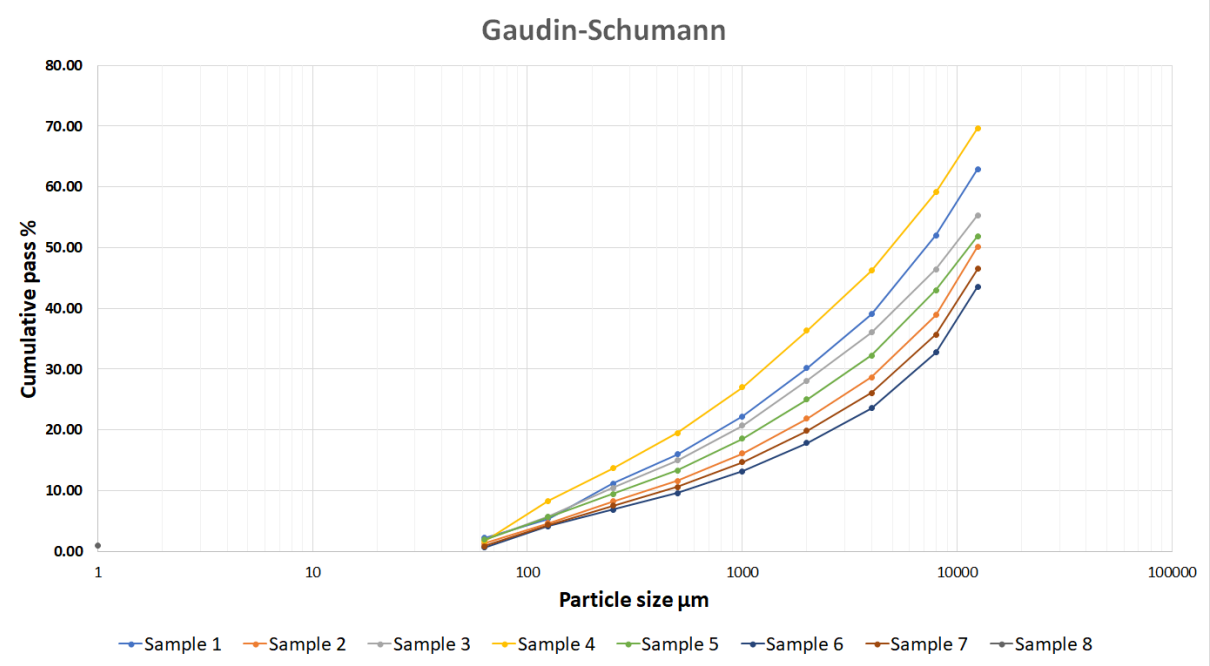

Fig. 6.1: Sieve analysis Gaudin-Schumann curve

increased when acid concentration was increased. Specially differences of copper and iron on $4.5g/l$ and $5.5g/l$ pf acid concentrations were rapidly increased. $Fe-S$ and $Fe-S-O$ forms of compounds are very active minerals which are easy to react. That is why iron concentration of pregnant solution was high. The solvent extraction (SX) process is stand for separate impurities (iron compounds and other metals) from copper in industry. Thus, if iron concentration of pregnant solution was high, cost of SX process would be increased.

In conclusion, economically and environmentally the best option of acid concentration is $4.5g/l$.

Acid concentration g/l	Element concentration, mg/l	
	Cu	Fe
2	123.7	172.4
2.5	145.8	206.9
3	173.0	232.4
3.5	162.2	225.0
4	157.0	234.2
4.5	189.1	260.0
5	168.5	244.1
5.5	193.8	284.5
6	183.8	294.8
6.5	204.4	357.0
7	198.3	328.4
7.5	194.2	334.9
8	175.5	316.4
8.5	210.4	349.3
9	207.3	353.9

Tab. 6.3: Vat leaching data

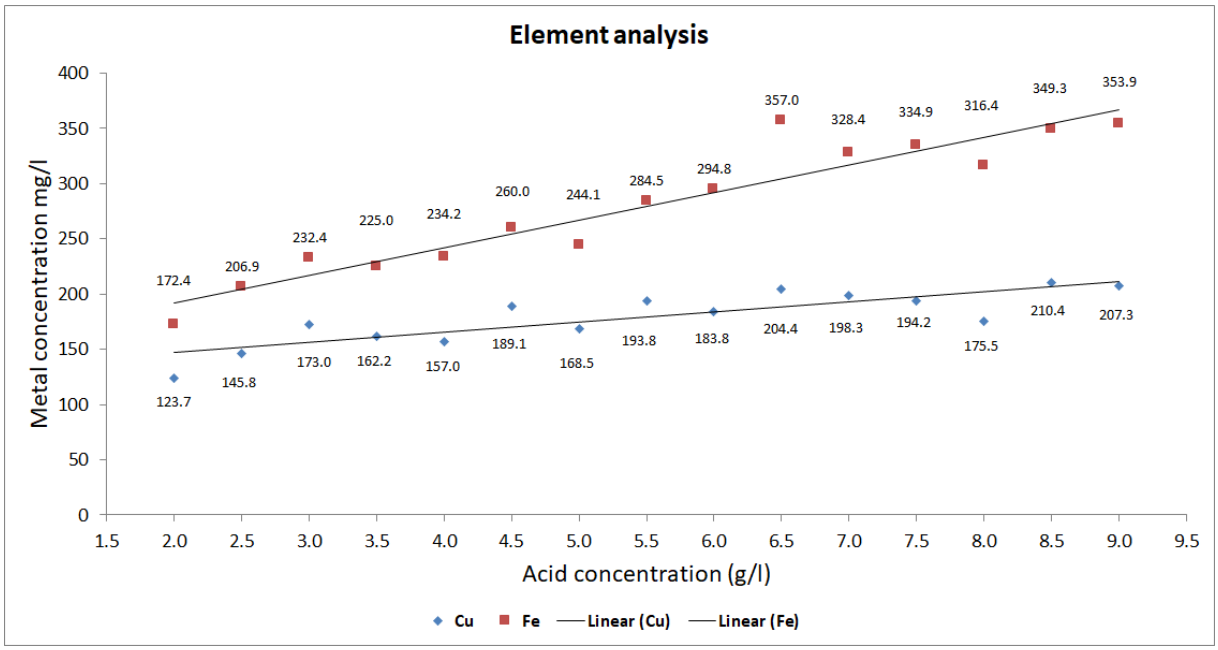

Fig. 6.2: Vat leaching

6.3 Column leaching

During 15 days, total acid consumption was 1131g, sodium hydroxide consumption was 880g and discharged pregnant solution was 359L (Table 6.4). From Figure 6.3, the second column had highest copper recovery rate which was also had highest flow rate, and the first column had lowest copper recovery rate which was also had lowest flow rate.

From Figure 6.3, we observed a same thing from all column, which was every recovery rates

jumped from zero to around 16% of recovery rate and then slowly increased from 16% to 34.1%. Thus, on second column, copper recovery rate jumped from 34.1% to 37.4% and then slowly increased.

		Column 1		Column 2		Column 3		Total NaOH	Description
Date	Time	Acid Consumption	Pregnant solution discharge (L)	Acid Consumption	Pregnant solution discharge (L)	Acid Consumption	Pregnant solution discharge (L)		
3/29/2019	9:00	60	-	60	-	60	-	0	
	21:00	-	-	-	-	-	-	0	
3/30/2019	9:00	-	-	-	-	-	-	0	
	21:00	-	-	-	-	-	-	0	
3/31/2019	9:00	-	-	30	18	-	5	56	
	21:00			30	7.5	15	3.7	27	
4/1/2019	9:00	-	2.1	15	8.5	15	4.2	36	
	21:00	-	1.9	30	7.5	15	3.3	31	
4/2/2019	9:00	15	2.2	30	8.6	15	4.5	37	
	21:00	-	2.2	30	4.7	15	4.5	28	
4/3/2019	11:00	-	2.7	-	9.2	15	5.3	42	
	21:00	24	1.8	27	7	24	3.95	31	
4/4/2019	9:00	-	2.2	-	8.75	-	5	39	Power shut
	21:00	-	2.1	45	8.05	15	4.7	36	Power shut
4/5/2019	9:00	-	-	-	-	-	-	0	Power shut
	21:00	48	2.4	36	5	48	5.1	31	
4/6/2019	9:00	-	2.3	-	4.9	-	3.2	25	
	21:00	-	2.2	-	7.3	-	4.85	35	
4/7/2019	9:00	-	2.2	30	7.9	-	4.5	36	
	21:00	-	2.05	30	4.25	30	4.3	26	
4/8/2019	9:00	-	2.25	12	8.4	12	4.7	38	
	21:00	-	2.15	-	8.15	-	4.65	37	
4/9/2019	9:00	30	2.65	45	10	30	5.1	43	
	21:00	-	1.9	-	7	-	4	32	
4/10/2019	9:00	45	2.85	75	10.8	60	6.1	48	
	21:00	-	1.6	-	5.2	-	3.9	26	
4/11/2019	9:00	-	2.4	-	3.8	-	5.1	28	2nd pump
	21:00	-	2.15	-	4	-	4.7	27	2nd pump
4/12/2019	9:00	-	2.25	15	8.5	-	4.9	38	
	21:00	30	2.7	15	10.2	-	5.5	45	
Total		252	51	555	193	369	115	880	

Tab. 6.4: Column leaching daily data

In conclusion about copper location, around 16% of total copper locates on surface of particles of ore samples which was type "a" and "b" of Table 2.1. Thus, 18.1% of total copper locates inside of rock and connected to surface via pores or crack like type "c" of Table 2.1. Approximately 3.3% of total copper was inside of rock and had crack or pores but did not reached the surface like type of "d" of Table 2.1. Thus, rest of total copper was located inside the particles and not connected to a pore like type "e" of Table 2.1.

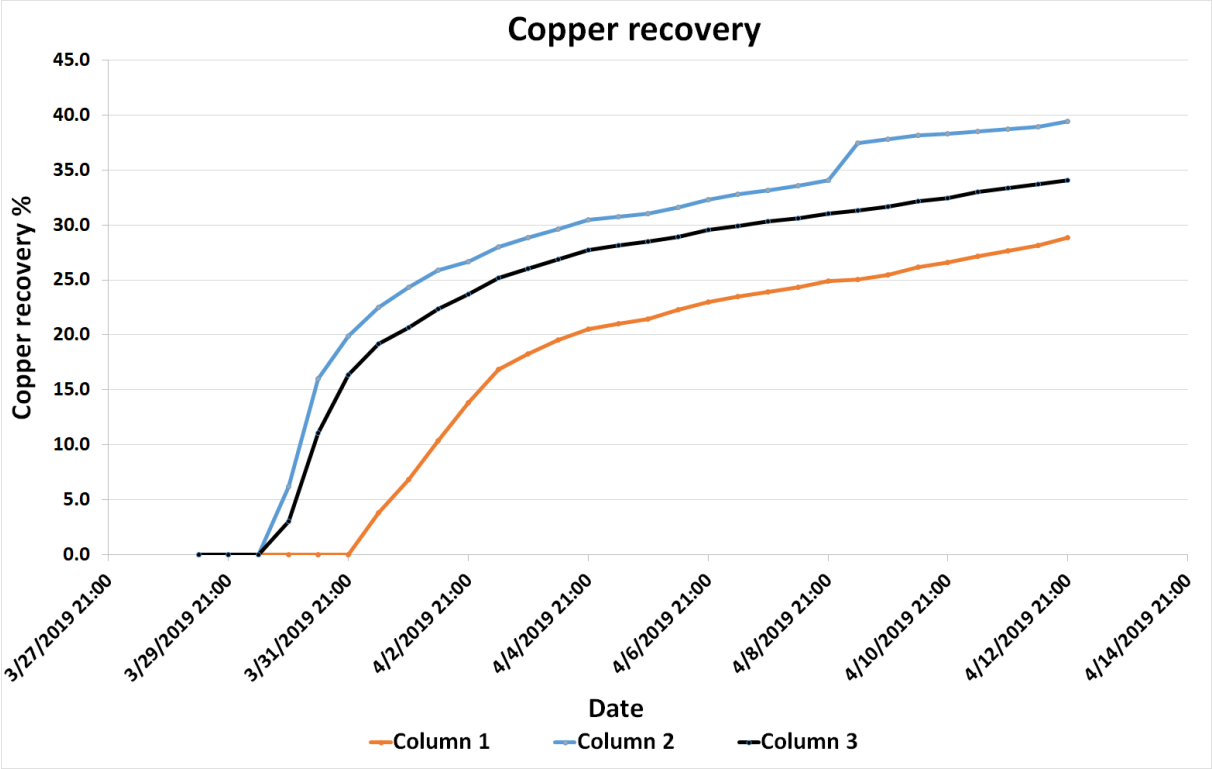

Fig. 6.3: Copper recoveries of column leaching

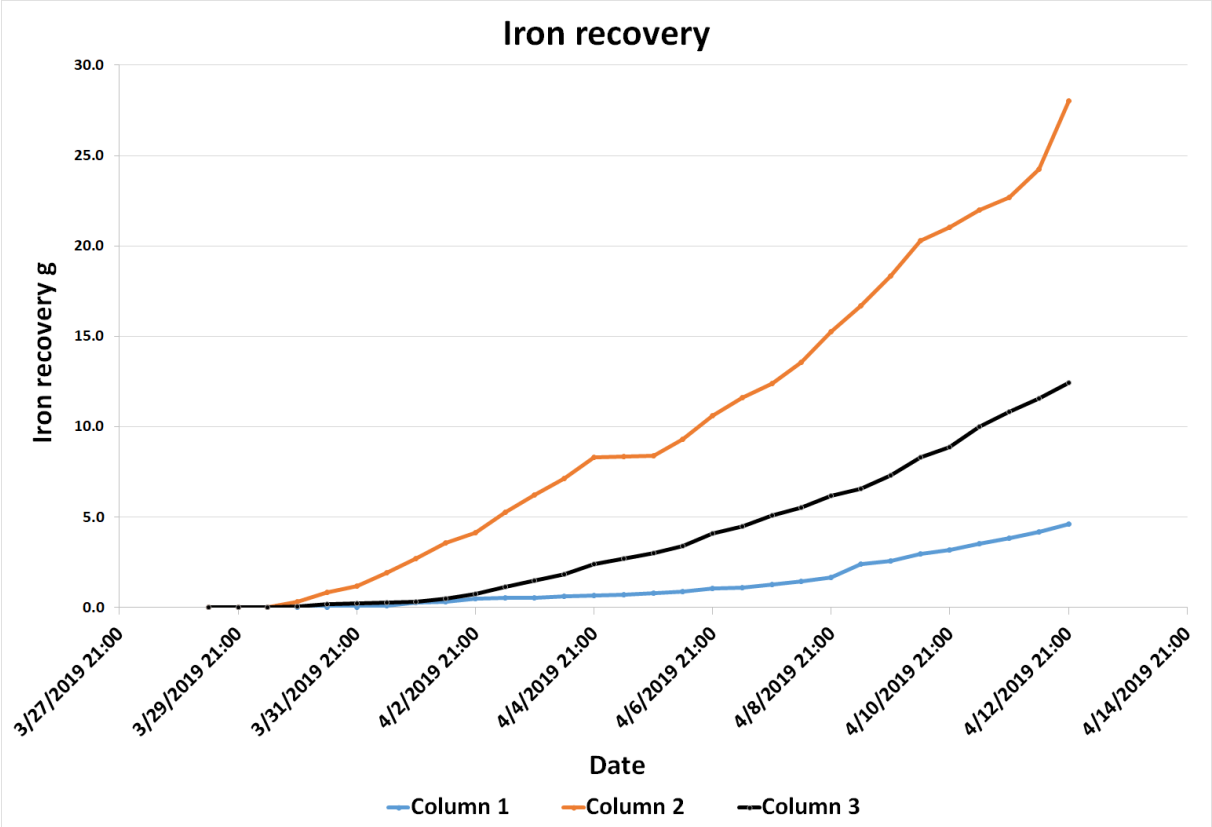

Fig. 6.4: Iron recoveries of column leaching

6.4 Simulation Result

Dissolution of rock by acid solution on the different time shown in Figures 6.5 and 6.6. The red color represent the highest and blue color represented the lowest dissolution parts. Solution slowly went down through the pores due to liquid head pressure and gravity, while dissolving metals. Theoretically, the top of ore dissolved more than bottom of ores, due to continuously solution feed. In other words, the column is identical with Continuous-Stirred-Tank-Reactor (CSTR). If CSTR's reaction time increased, then product's concentration would be increased. So that the reaction time of top of ore is longest which means kinetic of Solid-Liquid dissolution increased and this process went under Equation (3.17).

From our results (Figure 6.5 and 6.6). We can see that top of ore colors were usually red and

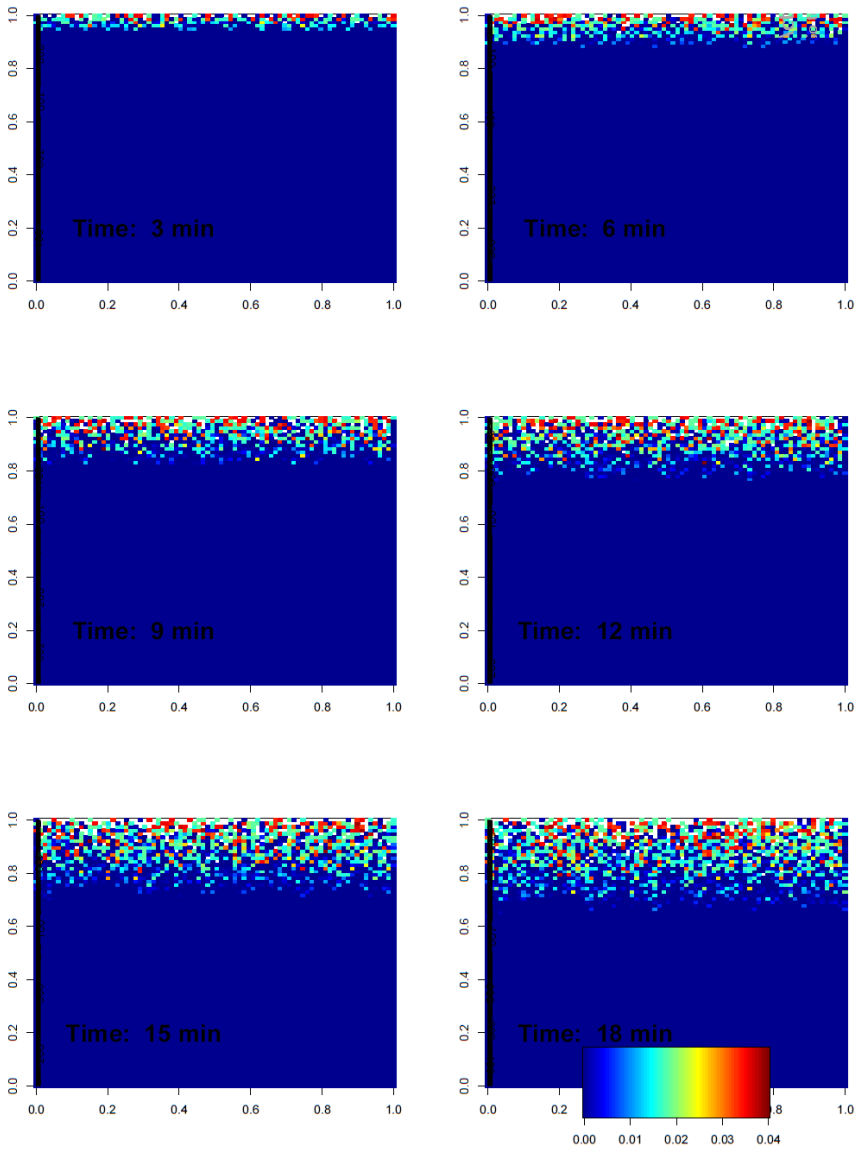

Fig. 6.5: First 16 minutes' of solution flow cross-section in column.

yellow which mean top of ore dissolved more. Thus theoretical approach and our forecasting column cross-sectional were matched.

We can see comparison of predicted and experimental recoveries in Figure 6.8. The squares,

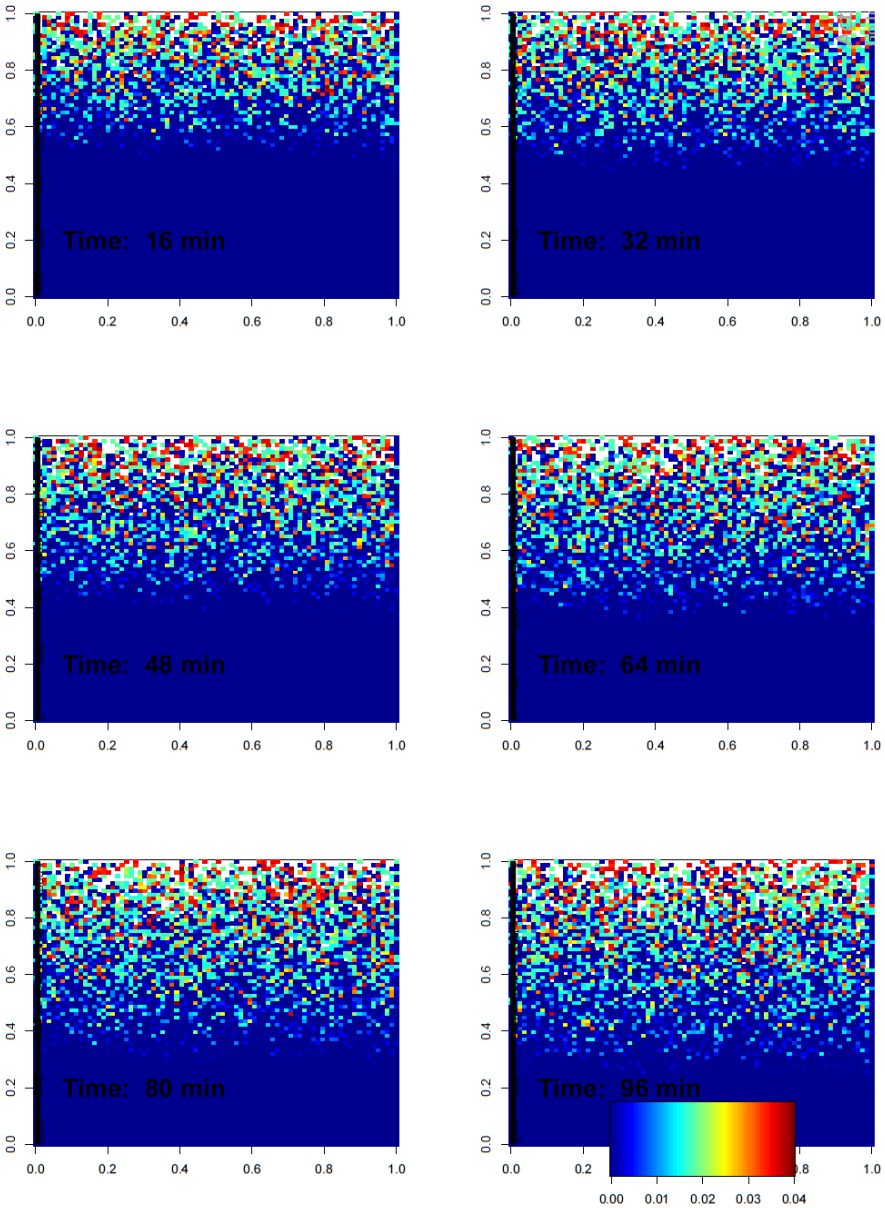

Fig. 6.6: Solution flow cross-section from 16 to 96 minutes in column.

triangles and circles were stands for representing experiment results and lines stands for representing predicted recoveries. On each columns, predicted and experimental recoveries' curves were almost same as each others. We calculated average and Roof-Mean-Square-Errors (RMSE) on Table 6.5.

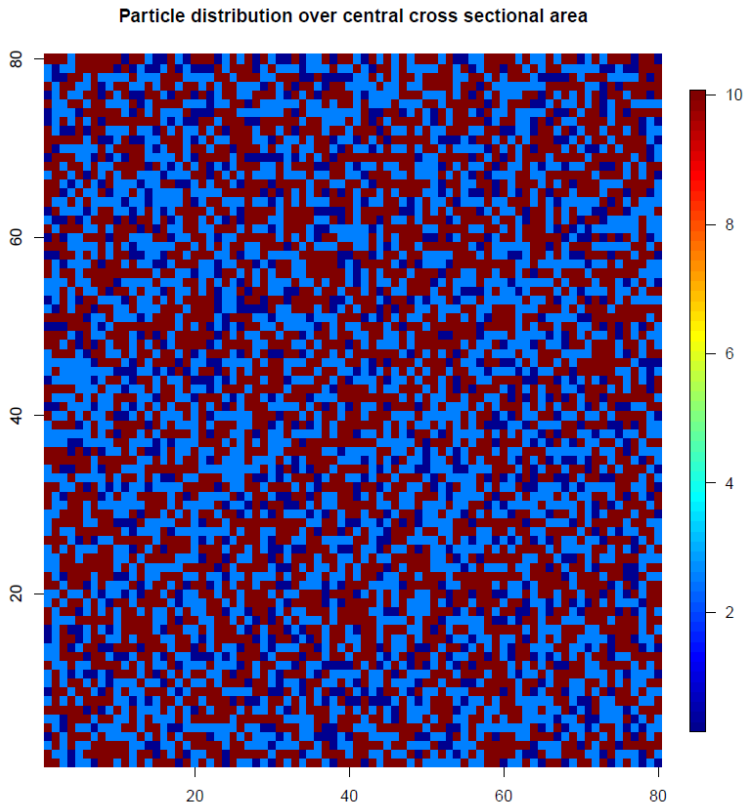

Fig. 6.7: Particle distribution over central cross sectional area.

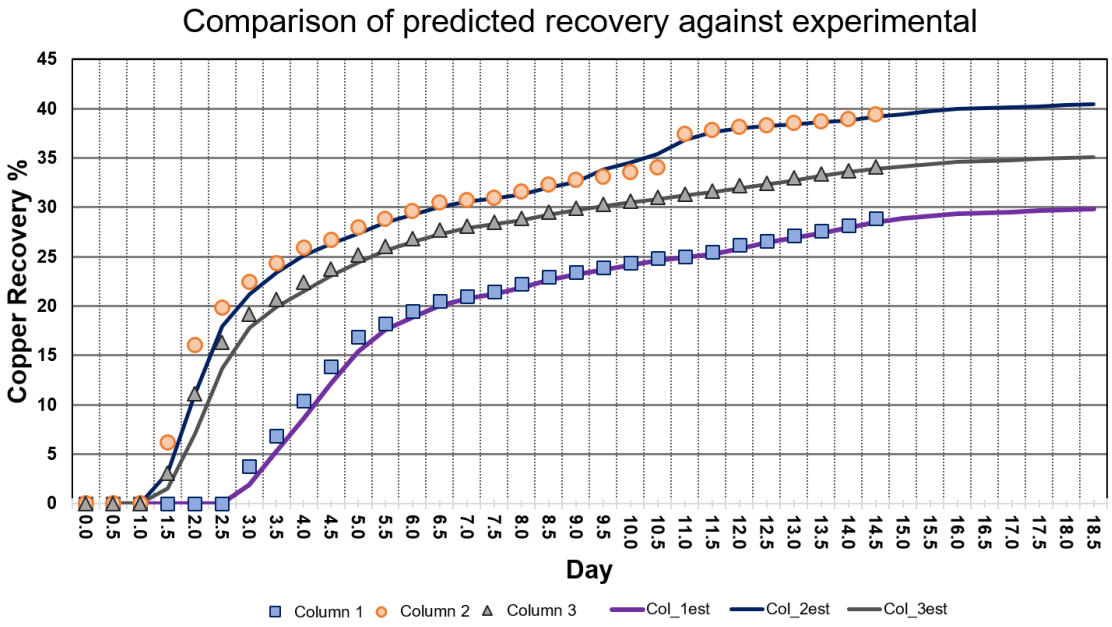

Fig. 6.8: Comparison of experimental and simulation results

Error analysis	Column 1	Column 2	Column 3	Total
Average error	0.497	0.723	0.588	0.603
RMSE	0.758	1.256	1.032	1.036

Tab. 6.5: Error analysis

7 Discussion and Conclusion

In this thesis, We simulated copper column leaching simulation. The vat and column leaching experiment were tested. Achit Ikht LLC supplied copper ore which was 2.22% copper concentrated. The column leaching experiment was tested for comparing to simulation results and finding relationship between metal recovery and flow rate of acid solution.

On the simulation section, Richard's equation (3.14) was considered as a main equation of fluid's flow direction through porous media and Finite Volume Method and Shrinking Core Models Equation (3.17) were used to dissolve of copper and iron.

From vat leaching experiment, the best acid concentration were $4.5g$ (Figure 6.2) on heap leaching. We observed that solution flow rate and metal recover were directly depends each other from column leaching experiment. The simulation result was approximately matched with experiment result (Figure 6.8). The average simulaiton error was 0.6% (Table 6.5) which means our simulation was worked correctly.

There are possibilities to continue my thesis by using more factors, which were gas flow, oxidation and precipitation, etc. on simulation for more accurate forecast results than in thesis's result.

8 Nomenclature

A	dimensionless	Experimentally calibrated mineral rate constant
B	dimensionless	Experimentally calibrated mineral rate constant
c_o	$mol \cdot m^{-3}$	Concentration of available reactant at particle surface
C_i	$mol \cdot m^{-3}$	Concentration of species i
D	$m^2 \cdot s^{-1}$	Dispersion coefficient
D_{eff}	$m^2 \cdot s^{-1}$	Effective rock diffusion coefficient
h	m	Liquid pressure head
H	m	Total hydraulic head
K	$m \cdot s^{-1}$	Hydraulic conductivity
K_c	dimensionless	Equilibrium constant
M_i	$kg \cdot mol^{-1}$	Molecular weight of the mineral
q	$m \cdot s^{-1}$	Darcy flux $q = -K(h)\nabla H$
r_o	m	Initial particle radius
r_m	m	Unreacted mineral radius
r_p	m	Mineral grain radius
R	$J \cdot mol^{-1} \cdot K^{-1}$	Universal gas constant
R_A, R_B	dimensionless	Adjustable rate parameters
t	s	Time
$t_e\sigma$	$S \cdot m^{-1}$	Electrical conductivity of the sulfur layer
T	K	Temperature
z	$m \cdot s^{-1}$	Gravity direction
a	dimensionless	Apparent activity that is based on bulk species concentration
β	dimensionless	Fraction of particle reacted
ΔG	$kJ \cdot mol^{-1}$	Free energy of the system
ε_g	$m^3 \cdot m^{-3}$	Volume fraction of the gas phase
ε_p	$m^3 \cdot m^{-3}$	Particle porosity
ζ	dimensionless	Shape factor for the mineral grain
θ	$m^3 \cdot m^{-3}$	Volume fraction of the liquid phase

Tab. 8.1: Nomenclature

9 Appendix

Date	Total Iron recovery, g			Total copper recovery g			Total copper recovery %		
	Column 1	Column 2	Column 3	Column 1	Column 2	Column 3	Column 1	Column 2	Column 3
3/29/2019 9:00	0.0	0.0	0.0	0.0	0.0	0.0	0.0	0.0	0.0
3/29/2019 21:00	0.0	0.0	0.0	0.0	0.0	0.0	0.0	0.0	0.0
3/30/2019 9:00	0.0	0.0	0.0	0.0	0.0	0.0	0.0	0.0	0.0
3/30/2019 21:00	0.0	0.3	0.0	0.0	13.9	6.8	0.0	6.2	3.0
3/31/2019 9:00	0.0	0.8	0.2	0.0	35.8	24.8	0.0	16.0	11.1
3/31/2019 21:00	0.0	1.2	0.2	0.0	44.4	36.5	0.0	19.9	16.3
4/1/2019 9:00	0.1	1.9	0.3	8.5	50.2	42.9	3.8	22.5	19.2
4/1/2019 21:00	0.3	2.7	0.3	15.3	54.4	46.1	6.8	24.3	20.6
4/2/2019 9:00	0.3	3.6	0.5	23.2	57.9	50.0	10.4	25.9	22.4
4/2/2019 21:00	0.5	4.1	0.7	31.0	59.6	53.0	13.9	26.7	23.7
4/3/2019 9:00	0.5	5.3	1.1	37.7	62.5	56.2	16.9	28.0	25.2
4/3/2019 21:00	0.5	6.2	1.5	40.8	64.5	58.2	18.3	28.9	26.1
4/4/2019 9:00	0.6	7.1	1.9	43.6	66.1	60.0	19.5	29.6	26.9
4/4/2019 21:00	0.7	8.3	2.4	45.9	68.1	61.9	20.5	30.5	27.7
4/5/2019 9:00	0.7	8.4	2.7	46.9	68.7	62.8	21.0	30.7	28.1
4/5/2019 21:00	0.8	8.4	3.0	47.9	69.3	63.7	21.5	31.0	28.5
4/6/2019 9:00	0.9	9.3	3.4	49.7	70.6	64.6	22.3	31.6	28.9
4/6/2019 21:00	1.0	10.6	4.1	51.4	72.3	66.0	23.0	32.3	29.6
4/7/2019 9:00	1.1	11.6	4.5	52.4	73.3	66.8	23.5	32.8	29.9
4/7/2019 21:00	1.3	12.4	5.1	53.4	74.1	67.8	23.9	33.1	30.3
4/8/2019 9:00	1.5	13.6	5.5	54.5	75.0	68.4	24.4	33.6	30.6
4/8/2019 21:00	1.7	15.2	6.2	55.6	76.1	69.4	24.9	34.1	31.1
4/9/2019 9:00	2.4	16.7	6.6	56.0	83.6	70.0	25.0	37.4	31.3
4/9/2019 21:00	2.6	18.3	7.3	56.9	84.5	70.8	25.5	37.8	31.7
4/10/2019 9:00	3.0	20.3	8.3	58.5	85.4	71.9	26.2	38.2	32.2
4/10/2019 21:00	3.2	21.0	8.9	59.5	85.6	72.5	26.6	38.3	32.4
4/11/2019 9:00	3.5	22.0	10.0	60.7	86.1	73.7	27.2	38.5	33.0
4/11/2019 21:00	3.8	22.7	10.8	61.8	86.5	74.6	27.6	38.7	33.4
4/12/2019 9:00	4.2	24.2	11.6	62.9	87.1	75.4	28.2	39.0	33.7
4/12/2019 21:00	4.6	28.0	12.4	64.5	88.2	76.2	28.8	39.5	34.1

Tab. 9.1: Copper and Iron recovery of column leaching

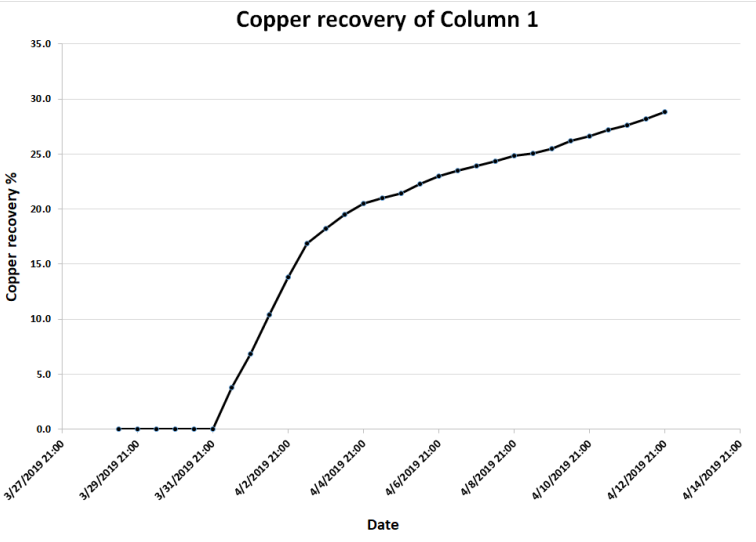

Fig. 9.1: Copper recovery of column one

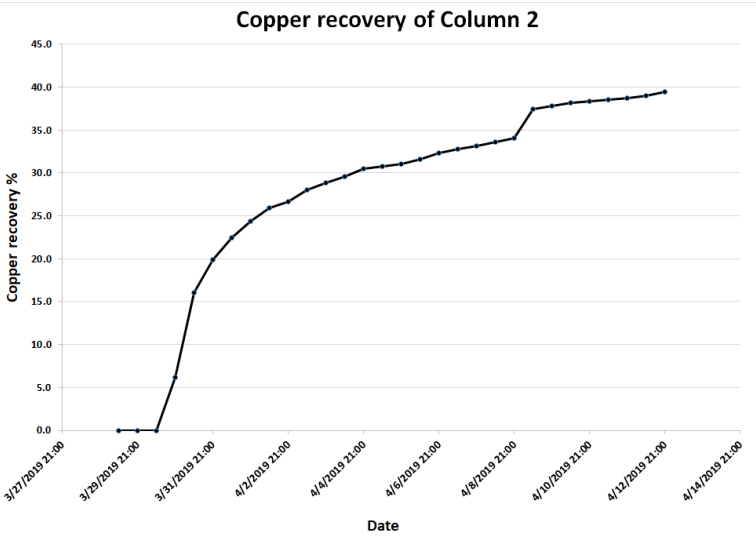

Fig. 9.2: Copper recovery of column two

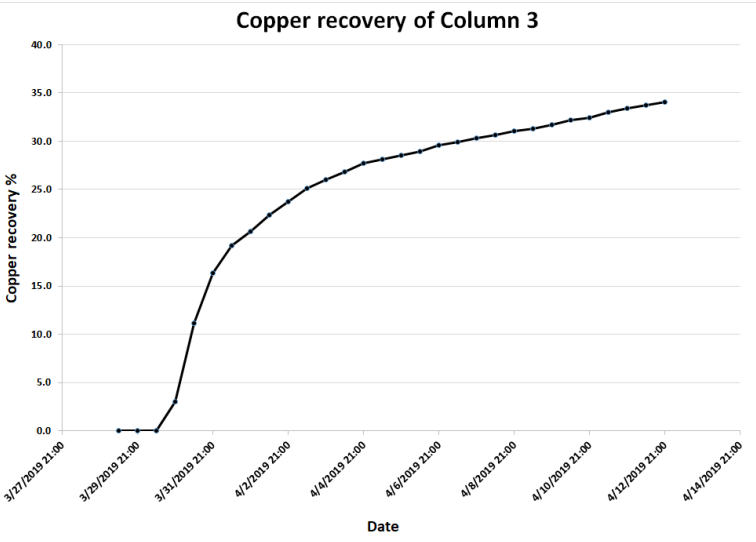

Fig. 9.3: Copper recovery of column three

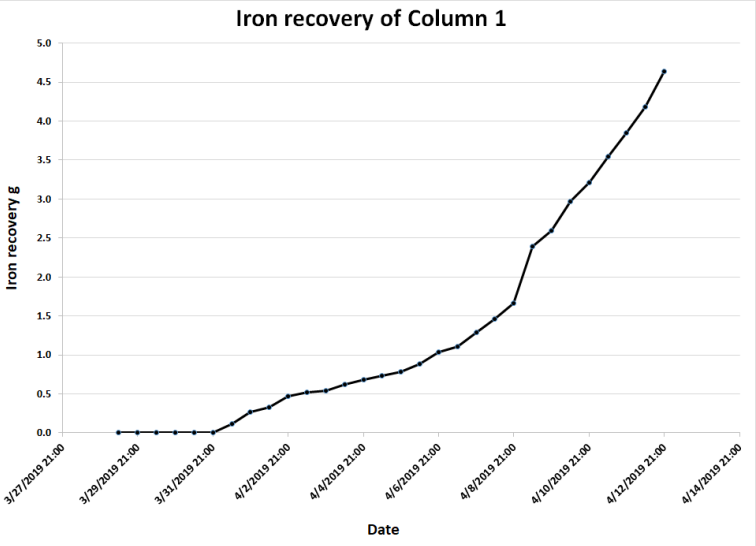

Fig. 9.4: Iron recovery of column one

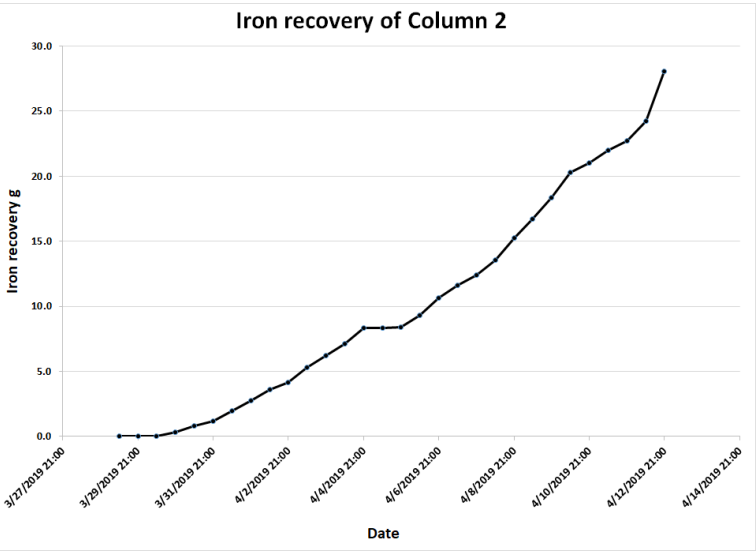

Fig. 9.5: Iron recovery of column two

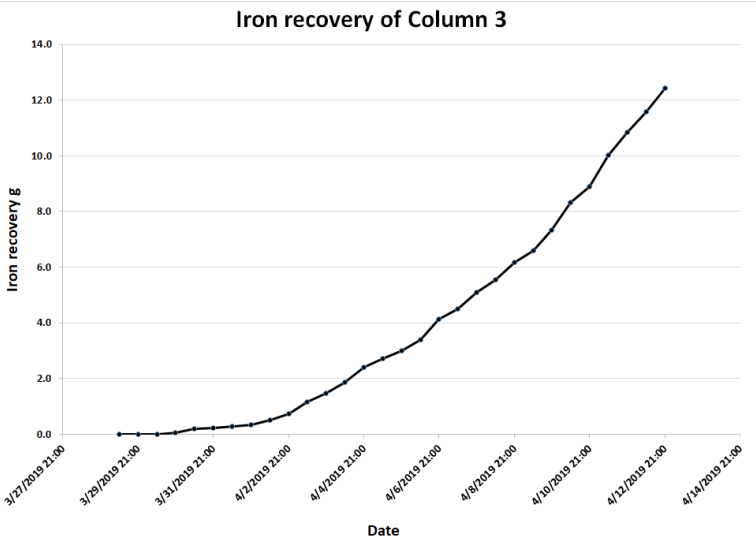

Fig. 9.6: Iron recovery of column three

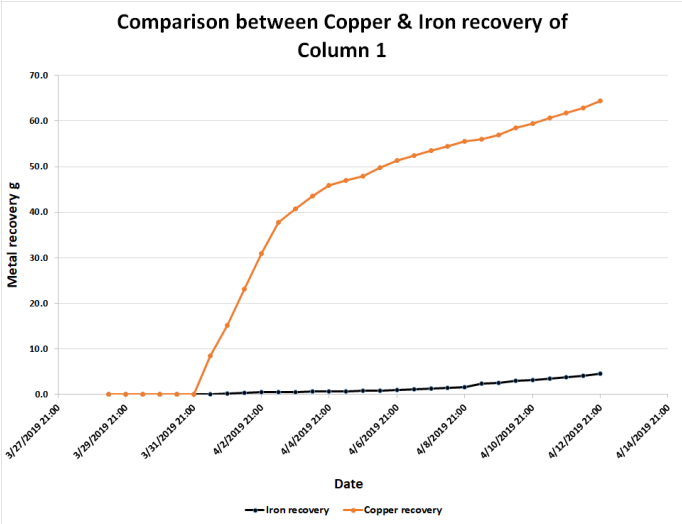

Fig. 9.7: Comparison of Copper and Iron recovery of column one

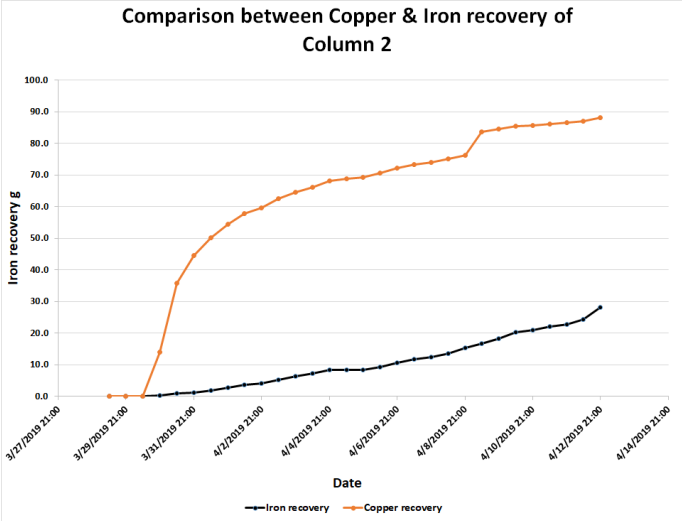

Fig. 9.8: Comparison of Copper and Iron recovery of column two

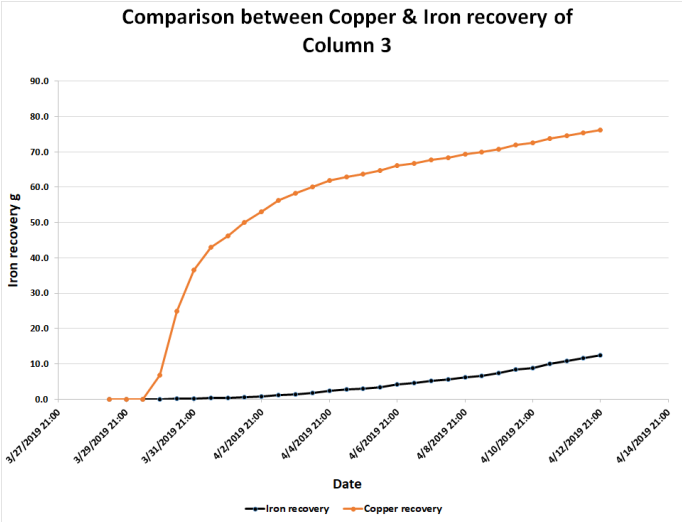

Fig. 9.9: Comparison of Copper and Iron recovery of column three

List of References

[1] Radetzki M. Seven thousand years in the service of humanity—the history of copper, the red metal. Resources Policy. 2009;34(4):176 – 184. Available from: http://www.sciencedirect.com/science/article/pii/S030142070900021X.

[2] Kelly TD, Matos GR. Historical statistics for mineral and material commodities in the United States. US Geological Survey Data Series 140. 2016;.

[3] Schlesinger ME, King MJ, Sole KC, Davenport WG. Chapter 1 - Overview. In: Schlesinger ME, King MJ, Sole KC, Davenport WG, editors. Extractive Metallurgy of Copper (Fifth Edition). fifth edition ed. Oxford: Elsevier; 2011. p. 1 – 12. Available from: http://www.sciencedirect.com/science/article/pii/B9780080967899100010.

[4] Ghorbani Y, Becker M, Mainza A, Franzidis JP, Petersen J. Large particle effects in chemical/biochemical heap leach processes – A review. Minerals Engineering. 2011;24(11):1172 – 1184. Special Issue : Bio and Hydrometallurgy. Available from: http://www.sciencedirect.com/science/article/pii/S0892687511001178.

[5] Kinnunen P. High-rate Ferric Sulfate Generation and Chalcopyrite Concentrate Leaching by Acidophilic Microorganisms. Tampere University of Technology; 2004. Available from: https://books.google.mn/books?id=zffzAgAACAAJ.

[6] Free ML. In: HYDROMETALLURGY: FUNDAMENTALS AND APPLICATIONS. Wiley; 2013. p. 146–152.

[7] Watling HR. The bioleaching of sulphide minerals with emphasis on copper sulphides — A review. Hydrometallurgy. 2006;84(1):81 – 108. Available from: http://www.sciencedirect.com/science/article/pii/S0304386X06001125.

[8] Jansen M, Taylor A. OVERVIEW OF GANGUE MINERALOGY ISSUES IN OXIDE COPPER HEAP LEACHING. 2003 01;.

[9] J Roman R, R Benner B, W Becker G. Diffusion Model for Heap Leaching and its Application to Scale-up. Trans Soc Min Eng AIME. 1974 09;256:247–252.

[10] Cathles L, Schlitt WJ. MODEL OF THE DUMP LEACHING PROCESS THAT INCORPORATES OXYGEN BALANCE, HEAT BALANCE, AND TWO DIMENSIONAL AIR CONVECTION. 1980;p. 9–27.

[11] Gao HW, Sohn HY, Wadsworth ME. A mathematical model for the solution mining of primary copper ore: Part II. leaching by solution containing oxygen bubbles. Metallurgical Transactions B. 1983 Dec;14(4):553–558. Available from: https://doi.org/10.1007/BF02653941.

[12] Bartlett RW. In: Solution mining : leaching and fluid recovery of materials. second edition ed. Amsterdam : Gordon and Breach Science Publishers; 1998. p. 341–368. Available from: http://hdl.loc.gov/loc.gdc/scd0001.00115284174.

[13] Marsden JO, Botz MM. Heap leach modeling — A review of approaches to metal production forecasting. Minerals & Metallurgical Processing. 2017 May;34(2):53–64. Available from: https://doi.org/10.19150/mmp.7505.

[14] McBride D, Gebhardt J, Croft N, Cross M. Heap Leaching: Modelling and Forecasting Using CFD Technology. Minerals. 2018 01;8:9.

[15] Angeli D, Amrit R, Rawlings JB. On average performance and stability of economic model predictive control. IEEE Trans on Automatic Control. 2012;57:1615–1626.

[16] McBride D, Ilankoon IMSK, Neethling SJ, Gebhardt JE, Cross M. Preferential flow behaviour in unsaturated packed beds and heaps: Incorporating into a CFD model. Hydrometallurgy. 2017;171:402 – 411. Available from: http://www.sciencedirect.com/science/article/pii/S0304386X16305461.

[17] Celia MA, Bouloutas ET, Zarba RL. A general mass-conservative numerical solution for the unsaturated flow equation. Water Resources Research;26(7):1483–1496. Available from: https://agupubs.onlinelibrary.wiley.com/doi/abs/10.1029/WR026i007p01483.

[18] Schaap M, Leij F. Improved prediction of unsaturated hydraulic conductivity with the Mualem-van Genuchten model. Soil Science Society of America Journal. 2000 5;64(3):843–851.

[19] McBride D, Cross M, Croft N, Bennett C, Gebhardt J. Computational modelling of variably saturated flow in porous media with complex three-dimensional geometries. International Journal for Numerical Methods in Fluids;50(9):1085–1117. Available from: https://onlinelibrary.wiley.com/doi/abs/10.1002/fld.1087.